J. metamorphic Geol., 1992, 10, 239–263

P–T evolution of the Teslin suture zone and Cassiar tectonites, Yukon, Canada: evidence for A- and B-type subduction

V. L. HANSEN
Department of Geological Sciences, Southern Methodist University, Dallas, TX 75275, USA

ABSTRACT Mineral composition and quantitative thermobarometric studies indicate that the Teslin-Taylor Mountain and Nisutlin terranes within the Teslin suture zone (TSZ), Yukon, record widespread high-P/T metamorphic conditions consistent with subduction zone dynamothermal metamorphism. The highest P–T conditions (575–750° C and 9–17 kbar) are preserved in tectonites formed during normal dip-slip ductile shear. Dextral strike-slip tectonites record lower P–T conditions (400–550° C and 5–8 kbar), and tectonites which show reverse shear have peak temperatures of *c.* 420° C and a minimum peak pressure of 3 kbar. Dynamothermal metamorphism took place in a west-dipping B-type subduction zone outboard of western North America in Permo-Triassic time. TSZ tectonites were underplated against the hangingwall plate of the subduction zone. Following subduction of the ocean basin which separated North America from the hangingwall plate, TSZ tectonites were overthrust eastward as a coherent structural package as a result of A-type subduction of Cassiar strata in early Jurassic time.

(Par)autochthonous Cassiar tectonites, which comprised the leading edge of the western North American margin, record prograde moderate-P, high-T metamorphism (550–750° C and 7–13 kbar) synchronous with top-to-the-east ductile shear. Metamorphism occurred as a result of subduction of the North American margin into the TSZ subduction zone in early Jurassic time. Following metamorphism Cassiar tectonites cooled slowly from 500 to 300° C during the period middle Jurassic to middle Cretaceous.

TSZ and Cassiar tectonites were deformed during changing P–T conditions. Data from each of these tectonite packages indicate that grain-scale strain partitioning may have allowed local recrystallization of individual minerals by the addition of mechanical energy. The composition of the new grains reflects the P–T conditions under which that particular grain was deformed.

Key words: dynamothermal metamorphism; high-P metamorphism; Permo-Triassic; subduction; thermobarometry; Yukon.

INTRODUCTION

The Teslin suture zone (TSZ), in southern Yukon, is the boundary between North American strata and accreted terranes in the northern North American Cordillera. The TSZ is juxtaposed against rocks of the (par)autochthonous Cassiar terrane, which is the Permo-Triassic margin of North American continental crust (Tempelman-Kluit, 1979; Hansen, 1989b). Both TSZ and Cassiar rocks in this region are L-S tectonites that record mid-crustal deformation. TSZ-related rocks extend south to the British Columbia border and north to east-central Alaska (Fig. 1). Cassiar rocks lie to the east in southern and central Yukon, and they are correlative with North American strata to the east and north. Based on regional geological, structural, and petrological evidence, several workers have proposed that the TSZ formed along a west-dipping convergent plate margin in Permo-Triassic time (Tempelman-Kluit, 1979; Erdmer, 1985; Hansen, 1987, 1988, 1989b). However, to date the only hard evidence that TSZ tectonites formed within a subduction environment lies in isolated eclogite blocks of uncertain structural context (Tempelman-Kluit, 1970; Erdmer & Helmstaedt, 1983; Erdmer, 1987). In addition, little is known about the metamorphic evolution of the Cassiar rocks and their role in terrane accretion. Armstrong (1988) postulated that these rocks were metamorphosed during a widespread mid-Cretaceous thermal event accompanied by plutonism. The metamorphism of both of these packages is important to our understanding of the Mesozoic evolution of the northern North American Cordillera and processes of terrane accretion, as they record Mesozoic dynamics along and outboard of the western North American margin.

In this paper I document the Mesozoic metamorphic evolution of TSZ and Cassiar terrane tectonites. Both packages record high-P/T dynamothermal metamorphic histories, yet the P–T–time–displacement paths for each tectonite package are quite different. TSZ tectonites were

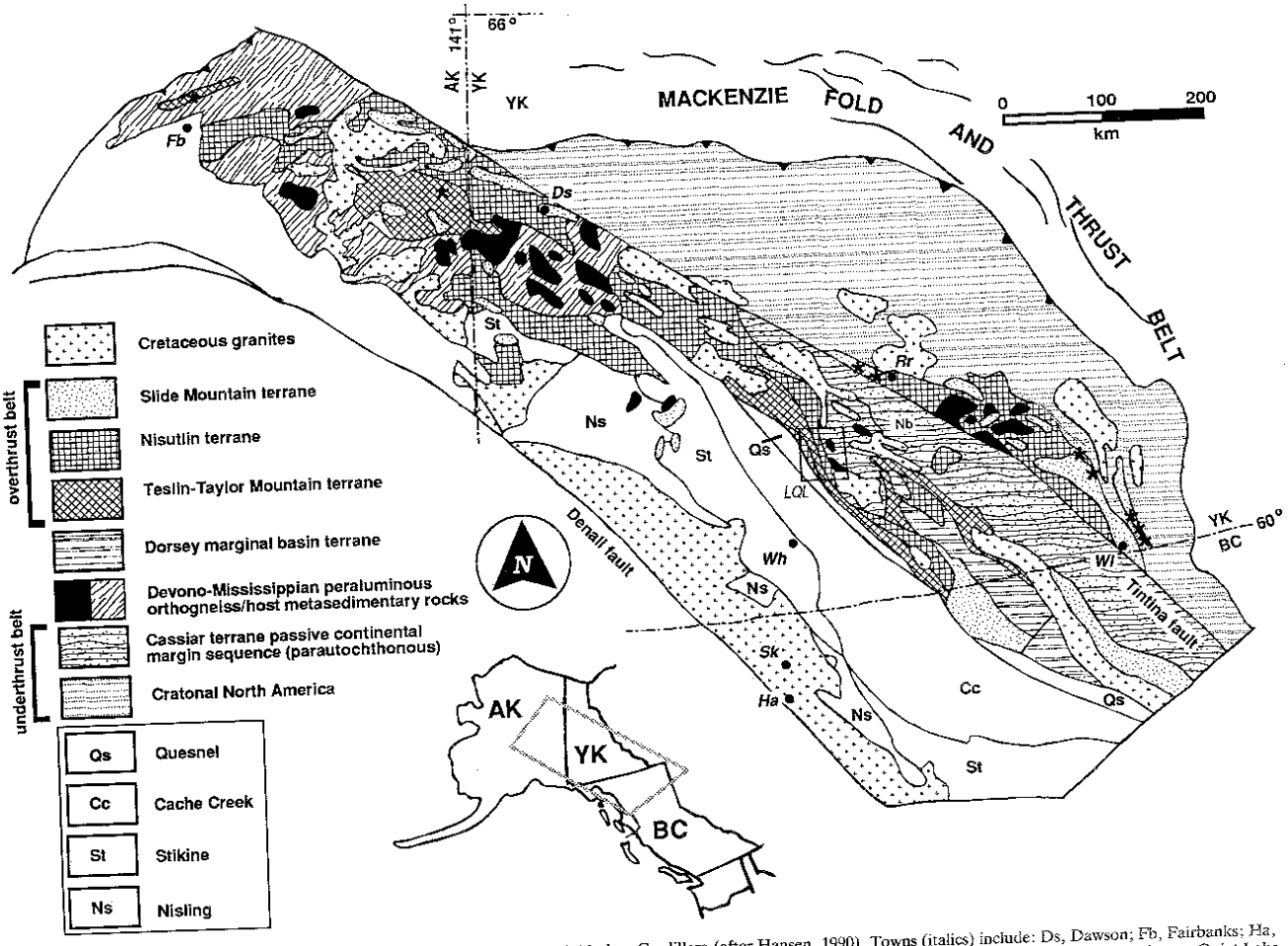

Fig. 1. Simplified terrane and subterrane map of the northern Canadian and Alaskan Cordillera (after Hansen, 1990). Towns (italics) include: Ds, Dawson; Fb, Fairbanks; Ha, Haines; Rr, Ross River; Sk, Skagway; Wh, Whitehorse; Wl, Watson Lake. The TSZ is the part of the Teslin-Taylor Mountain and Nisutlin terranes in the Laberge–Quiet Lake (LQL) area (box). Approximate location of figure shown on inset map.

metamorphosed as a coherent belt under high-P/T conditions when they were underplated onto the hangingwall of a west-dipping B-type subduction complex. A B-subduction zone is one along which oceanic lithosphere is subducted in contrast with A-subduction in which continental lithosphere is subducted (cf. Bally, 1981). The TSZ was thrust eastward over the North American continental margin in early Jurassic time, resulting in collision and accretion to North America. In contrast, Cassiar tectonites, which represent the leading edge of North American continental crust, experienced high-P/T metamorphism as a result of A-type subduction. The TSZ and Cassiar terrane comprise a pair of high-P/T tectonite belts which record B-type subduction prior to collision and A-type subduction as a result of subduction of North American continental crust, respectively. The record of subduction zone deformation and metamorphism is partly obscured by subduction-related strike-slip faulting, and by collision of the TSZ with the North American continental margin, which resulted in the accretion of TSZ tectonites to the subducting footwall plate.

This paper is divided into two parts. The first part presents quantitative P–T constraints on the conditions of deformation of each tectonite package and discusses the implications of these data for the effect of strain partitioning on grain-scale chemical equilibrium in L-S tectonites in general. The second part combines P–T constraints with existing age and structural data in order to reconstruct P–T–time–displacement paths for the individual tectonite domains, and in it the regional tectonic implications of these deduced paths is briefly discussed.

TECTONIC SETTING

The Slide Mountain, Teslin-Taylor Mountain, and Nisutlin terranes, which lie structurally upon parautochthonous (Cassiar terrane) to autochthonous Lower Jurassic or older North American strata, comprise the easternmost accreted terranes in the northern Cordillera (Fig. 1). These three terranes are referred to as the overthrust assemblage, and Cassiar and North American strata are referred to as the underthrust assemblage. The overthrust assemblage was emplaced in late Triassic to late Jurassic time (Tempelman-Kluit, 1979). A sliver of the overthrust assemblage, together with its (par)autochthonous substrate, was offset approximately 450 km by post-Jurassic dextral displacement along the Tintina fault (Roddick, 1967; Tempelman-Kluit, 1979). Both the overthrust and underthrust assemblages are dissected by high-angle dextral strike-slip zones, and they are intruded by mid-Cretaceous plutons (Gabrielse, 1985).

The Slide Mountain terrane, generally the easternmost accreted terrane, is composed of imbricate fault slices of weakly metamorphosed Devonian to Triassic oceanic strata and Permian to Triassic arc-related strata (Harms, 1985; Nelson & Bradford, 1987; Nelson *et al.*, 1988). Displacement, along low-angle faults, is generally orogen-normal with continentward vergence, although orogen-parallel displacement is seen locally (Nelson *et al.*, 1988; Nelson, 1990). Imbrication of the Slide Mountain terrane occurred prior to late Triassic–early Jurassic emplacement onto autochthonous lower-plate strata (Gordey *et al.*, 1982; Harms, 1985).

The Teslin-Taylor Mountain and Nisutlin terranes are composed of dynamothermally metamorphosed sedimentary, volcanic and plutonic rocks characterized by an L-S tectonite fabric. Teslin-Taylor Mountain protoliths include metamafic and metasiliceous oceanic rock types which are correlative with Slide Mountain lithologies (Hansen, 1987, 1988, 1990; Wheeler *et al.*, 1988). Nisutlin rocks are dominantly quartz-rich clastic metasedimentary rocks. Together the Teslin-Taylor Mountain and Nisutlin tectonites form a zone of gently dipping tectonites in east-central Alaska and western Yukon, which tapers into the relatively narrow TSZ in southern Yukon. In the TSZ, tectonite foliation strikes NNW and dips moderately to steeply west, parallel to the trend of the zone (Fig. 1). The Teslin-Taylor Mountain and Slide Mountain terranes represent different structural levels of a collapsed marginal ocean basin, and Nisutlin protoliths represent marginal clastic sediments (Hansen, 1988, 1990; Wheeler *et al.*, 1988).

The underthrust assemblage is composed of (par)autochthonous continental-margin strata of the Cassiar terrane and/or ancestral western North America (Wheeler *et al.*, 1988). These rocks range in metamorphic grade from unmetamorphosed to amphibolite facies. L-S tectonite fabrics characterize amphibolite-grade Cassiar rocks, which include Devonian–Lower Carboniferous orthogneiss that records Proterozoic U–Pb inheritance and Sm–Nd model ages similar to North American cratonic basement values (Bennett & Hansen, 1988; Hansen *et al.*, 1989).

GEOLOGICAL AND STRUCTURAL RELATIONS

The eastern Laberge–western Quiet Lake area, southern Yukon, provides the best continuous exposure of TSZ tectonites and Cassiar tectonites. The TSZ exposes a 15–20-km-thick structural section. Geological and structural relations are summarized from Hansen (1989b).

The region is divisible into three north-trending structural belts (Fig. 2). West of the Big Salmon fault mainly Lower Carboniferous non-metamorphosed or low-grade volcanic, volcaniclastic and sedimentary rocks of the Quesnel terrane (Wheeler *et al.*, 1988) are cut by extensive NNW-striking, high-angle faults. L-S tectonites of the TSZ comprise a steeply dipping rock package between the Big Salmon and the d'Abbadie faults. Metamorphic grade ranges from albite–epidote amphibolite and rare eclogite facies in the west, to greenschist facies in the east. Tectonites include rocks of the Teslin-Taylor Mountain, Nisutlin and, locally, Cassiar terranes. East of the d'Abbadie fault the Teslin-Taylor Mountain and Nisutlin tectonites lie in klippen above Cassiar paragneiss and orthogneiss. Typically concordant

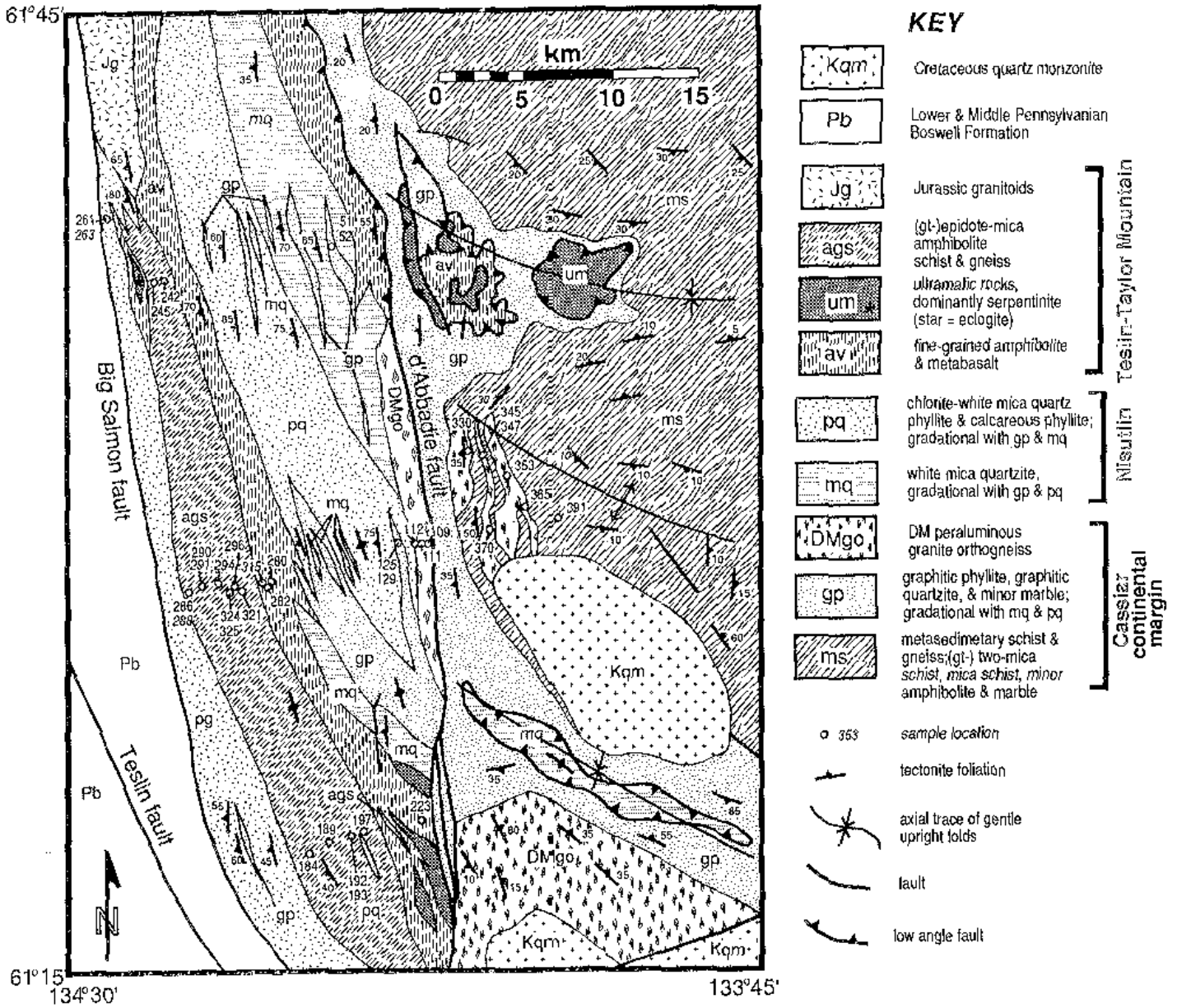

Fig. 2. Simplified geological map of the Laberge–Quiet Lake area showing location of samples for thermobarometric analysis (after Hansen, 1989b).

foliation in the *klippen and underlying tectonites marks* gentle, upright, gently plunging folds with NW-striking *axial surfaces. Klippen are generally preserved within the* synforms, whereas the antiforms expose Cassiar *tectonites.*

The d'Abbadie fault, which separates steeply west-*dipping* tectonites to the west from gently dipping tectonites to the east, post-dates late Cretaceous dextral ductile shear (Hansen *et al.*, 1991). Upper Cretaceous granitic plutons intrude the d'Abbadie fault. Neither the sense nor the amount of displacement associated with brittle deformation along the d'Abbadie, Big Salmon and Teslin faults are known.

Rocks on either side of the d'Abbadie fault are L-S tectonites. West of the d'Abbadie fault TSZ foliation dips steeply in the west and becomes shallow in the east. The TSZ is itself divisible into three structural domains on the *base of differently orientated elongation lineation*, Le (Fig. 3). From west to east, these are: (1) D_{Nds}, which comprises a 5–8-km-wide zone of top-to-the-WSW, or apparent right-normal oblique shear; (2) D_{Dss}, which marks a 1–2-km-thick zone of dextral strike-slip shear; and (3) D_{Rds}, a 1–10-km-wide zone of top-to-the-SE, or apparent right-reverse oblique shear. Nds identifies normal-sense dip-slip displacement, Dss dextral strike-slip and Rds reverse dip-slip. I refer to these three domains collectively as the TSZ tectonites. Ductile deformation of the TSZ tectonites occurred prior to rapid cooling in early Jurassic time as shown by $^{40}Ar/^{39}Ar$ mineral age data (Hansen *et al.*, 1991). L-S tectonites adjacent to the d'Abbadie fault record dextral strike-slip shear. Although these tectonites appear correlative with D_{Dss} tectonites on the basis of structural geometry and kinematic data, they include an orthogneiss unit that records late Cretaceous

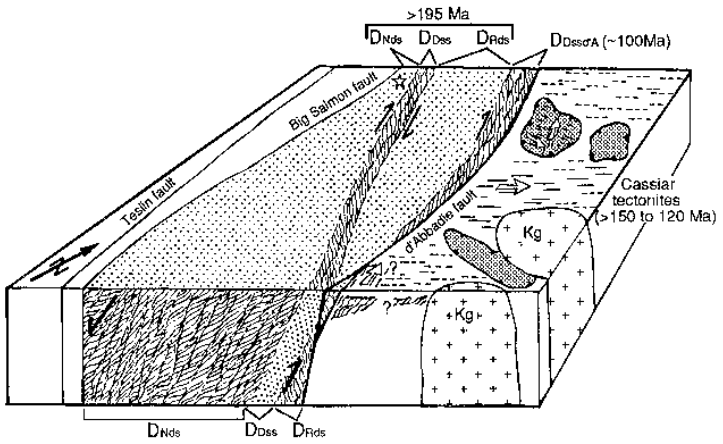

Fig. 3. Schematic block diagram of the Laberge–Quiet Lake map area (Fig. 2) showing kinematic interpretation and $^{40}Ar/^{39}Ar$ cooling dates (Hansen, 1989b; Hansen *et al.*, 1991). D_{Nds} identifies normal-sense dip-slip shear, D_{Dss} dextral strike-slip shear, D_{Rds} reverse dip-slip shear, and $D_{Dssd'A}$ dextral strike-slip shear parallel with the d'Abbadie fault.

dextral shear (*c.* 97 Ma), and they are assigned to a separate domain, $D_{Dssd'A}$. Dss stands for dextral strike-slip displacement and d'A indicates parallelism with the d'Abbadie fault. East of the d'Abbadie fault, paragneiss and orthogneiss of the Cassiar terrane record top-to-the-east ductile shear, and are referred to as Cassiar tectonites. Although Cassiar tectonites record top-to-the-east dip-slip shear similar to D_{Rds} tectonite of the TSZ, they record slow cooling between 500 and 300° C between the late Jurassic and middle Cretaceous (*c.* 150–109 Ma; Hansen *et al.*, 1991).

P–T CONDITIONS

The grade of metamorphism in Teslin-Taylor Mountain and Nisutlin rocks varies from albite–epidote amphibolite facies in rocks in the west, to blueschist and greenschist facies preserved in klippen to the east; eclogite blocks are preserved locally (Tempelman-Kluit, 1970, 1979; Gordey, 1981; Erdmer & Helmstaedt, 1983; Mortensen, 1983; Erdmer, 1987). Metamorphic grade across the TSZ ranges from albite–epidote amphibolite facies with rare eclogite blocks in the west, to greenschist facies in the east (Tempelman-Kluit, 1979; Erdmer, 1985; Hansen, 1987).

Amphibolite, pelitic schist, calc-silicate gneiss and orthogneiss are the rock types most useful for constraining *P–T* conditions within the study area. Micaceous quartzite, graphitic quartzite, calcareous phyllitic quartzite and marble comprise much of the TSZ. The interlayering of rock types and the structural and kinematic signature of TSZ tectonites allow extrapolation of metamorphic facies and *P–T* conditions over a broad area. Coexistence of albite, epidote and hornblende in amphibolite indicates that moderately high-*P/T* metamorphic conditions (Apted & Liou, 1983; Maruyama *et al.*, 1983) accompanied both D_{Nds} and D_{Dss} tectonism. Orthogneiss, calc-silicate gneiss and pelitic schist have no minerals that constrain pressure.

Because of the limited applicability of phase relations in these rocks, *P–T* constraints were derived qualitatively by mineral chemistry and quantitatively by thermobarometry. Constraints are provided by: (1) amphibole composition; (2) garnet–biotite, garnet–hornblende and calcite–dolomite thermometry; (3) garnet–biotite–muscovite–plagioclase, garnet–plagioclase and garnet–hornblende–plagioclase barometry; and (4) white mica composition. Coupled with tectonite fabric relations and age data, these *P–T* estimates are used to trace the evolution of these rocks through time and space. For example, although both D_{Nds} and D_{Dss} tectonites contain albite–epidote amphibolite facies assemblages, their mineral compositions reveal significant *P–T* changes from the formation of pervasive D_{Nds} fabrics to localized D_{Dss} fabric zones.

Electron microprobe analyses

Samples used for calcite–dolomite thermometry were analysed on an ARL-EMX electron microprobe equipped with automated crystal spectrometers and Tracor-Northern NS-880 energy- and wavelength-dispersive systems. Analyses were obtained with a sample current of approximately 18 nA, accelerating voltage of 15 kV, and a defocused spot diameter of 10–15 μm. Synthetic and natural minerals standards were analysed before, during and after each sample suite in order to monitor drift. Data were reduced on-line using the alpha correction factors of Albee & Ray (1970). Control standards showed a reproducibility of ±2% for major elements and ±10% for minor elements.

All other samples were analysed using an automated Cameca CMB electron microprobe, with a sample current of approximately 18 nA and accelerating voltage of 15 kV. Ten-oxide analyses were performed using a minimum beam diameter of 2–4 μm for all phases, except for micas, for which a slightly broader beam was used. Data were reduced on-line using the ZAF correction scheme. Analysis of synthetic and natural mineral standards was reproducible to better than ±2% for major elements and ±10% for minor elements. Most analyses reported represent an average of three or more individual spot analyses and are therefore more precise (approximately

±1% for major elements). Analyses are given in Table 1 and Tables 3–8. Spot-analysis traverses were made to check for zonation in garnet, plagioclase, hornblende and mica.

Amphibole analyses were recalculated using the algorithm of Laird & Albee (1981a) to estimate Fe^{3+}/Fe^{2+} ratios. The minimum Fe^{3+} consistent with stoichiometry is reported in this study. Iron in chlorite, garnet and biotite was assumed to be all ferrous. Iron in plagioclase and epidote was assumed to be all ferric. Iron in white mica analyses was assumed to be all ferrous, except where noted as recalculated using the algorithm of Laird & Albee (1981a) to estimate Fe^{3+}/Fe^{2+} ratios.

Amphibole chemistry

The Ti content of hornblende, in the presence of a Ti-rich phase such as rutile, ilmenite or titanite, increases with increasing metamorphic grade (Rasse, 1974; Spear, 1981). Ti content in D_{Nds} and D_{Dss} hornblende defines two overlapping populations, indicating qualitatively higher metamorphic temperatures for D_{Nds} (Fig. 4).

The compositional variation of amphibole within mafic schist containing the common assemblage Ca-amphibole + Ep + Pl + Chl + Ti phase ± Fe-oxide ± Wm ± Qtz reflects the metamorphic environment of formation (Laird & Albee, 1981a, b). Actinolite, the stable amphibole in the greenschist facies, grades compositionally toward tschermakite and edenite through $Al^{vi}Al^{iv}(Fe, Mg)_{-1}Si_{-1}$ and $NaAl^{iv}[\,]_{-1}Si_{-1}$ substitutions, respectively, in the amphibolite facies, and toward glaucophane through $NaAl^{vi}Ca_{-1}(Fe, Mg)_{-1}$ substitution in the blueschist facies. Laird & Albee (1981a, b) constructed a series of compositional plots, based on amphibole site occupancy, which discriminate four petrotectonic environments of amphibole formation marked by widely varying P–T conditions. The compositional variation of Ca-amphibole in TSZ mafic tectonites is primarily a function of tschermak, pargasite and glaucophane substitution (Fig. 5). The amphiboles plot chiefly within the Sanbagawa and Franciscan field of Laird & Albee (1981a, b); therefore, TSZ metamorphism is consistent with high-P, intermediate-T metamorphism (Miyashiro, 1961), such as in a subduction zone environment (Ernst, 1975).

Although TSZ amphiboles in general show substitution similar to Sanbagawa and Franciscan amphiboles, D_{Nds} and D_{Dss} amphiboles have distinct compositions. D_{Nds} amphiboles show greater enrichment in glaucophane and, to a lesser extent, tschermak components than D_{Dss} amphiboles (Fig. 5b-d), and reflect qualitatively higher P–T conditions. Na^{M4} site occupancy, which increases with pressure (Brown, 1977), is greater for D_{Nds} tectonites.

Sample DW-280, a D_{Dss} amphibolite tectonite, contains two texturally and compositionally distinct types of amphibole (Table 1). Coarse-grained and fine-grained (locally as rim overgrowths on coarse grains) amphiboles plot within the D_{Nds} and D_{Dss} fields, respectively, on amphibole discrimination diagrams (Fig. 5), and are interpreted to represent progressive metamorphic conditions during D_{Nds} and D_{Dss}. During D_{Dss}, grain-scale strain partitioning may have allowed localized recrystallization of individual minerals by the addition of mechanical energy, thereby permitting a portion of the coarse-grained amphibole to recrystallize with a new composition reflecting the metamorphic conditions associated with D_{Dss}. If local equilibrium existed on the scale of a few grains, it is possible that different minerals or suites of minerals formed during heterogeneous ductile strain may record successive points along the P–T evolution of a dynamically recrystallizing rock. If so, additional analysis of individual grains may reveal compositions indicative of changing P–T conditions during deformation.

These compositional data indicate that: (1) TSZ D_{Nds} and D_{Dss} tectonites were metamorphosed at high pressure, consistent with metamorphism within a subduction zone environment; and (2) D_{Nds} deformation took place at generally higher P–T than D_{Dss}.

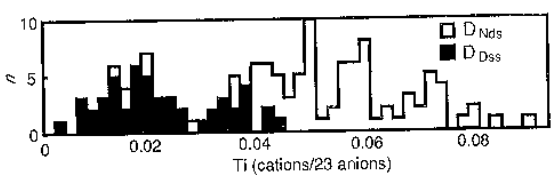

Fig. 4. Plot of Ti content in amphibole in the assemblage amphibole + Ep + Pl + Chl + a Ti phase ± Fe-oxide ± Wm ± Qtz. D_{Nds} amphiboles display higher Ti content than D_{Dss} amphiboles, which indicates a higher grade of metamorphism. n = number of analyses.

Thermobarometry

Four rock types were used for thermobarometric analysis (Table 2); the locations of samples are shown on Fig. 2. Metacarbonates yielded temperatures based on calcite–dolomite/Ca–Mg exchange thermometry. Thermobarometers based on cation exchange among garnet–biotite, garnet–biotite–plagioclase and garnet–biotite–muscovite–plagioclase were applied to garnet mica schist, and white mica composition constrains metamorphic pressure in two-mica quartzofeldspathic schists and orthogneiss. Garnet–hornblende and garnet–hornblende–plagioclase exchange thermobarometers were used to constrain amphibolite P–T conditions. A lack of aluminium silicate polymorphs in these Al-deficient tectonites precluded the use of other thermobarometers.

Calcite–dolomite assemblages have only been found in D_{Rds} and $D_{Dssd'A}$ tectonites adjacent to the d'Abbadie fault. Assemblages necessary for garnet–biotite–muscovite–plagioclase thermobarometry were found within D_{Nds}, D_{Dss} and Cassiar tectonites; however, assemblages for garnet–hornblende–plagioclase thermobarometry have only been found in D_{Nds} tectonites. White mica barometry was applied to D_{Nds}, D_{Dss}, $D_{Dssd'A}$ and Cassiar tectonites.

Thermobarometric calculations are based on the compositions of minerals in contact and interpreted to be

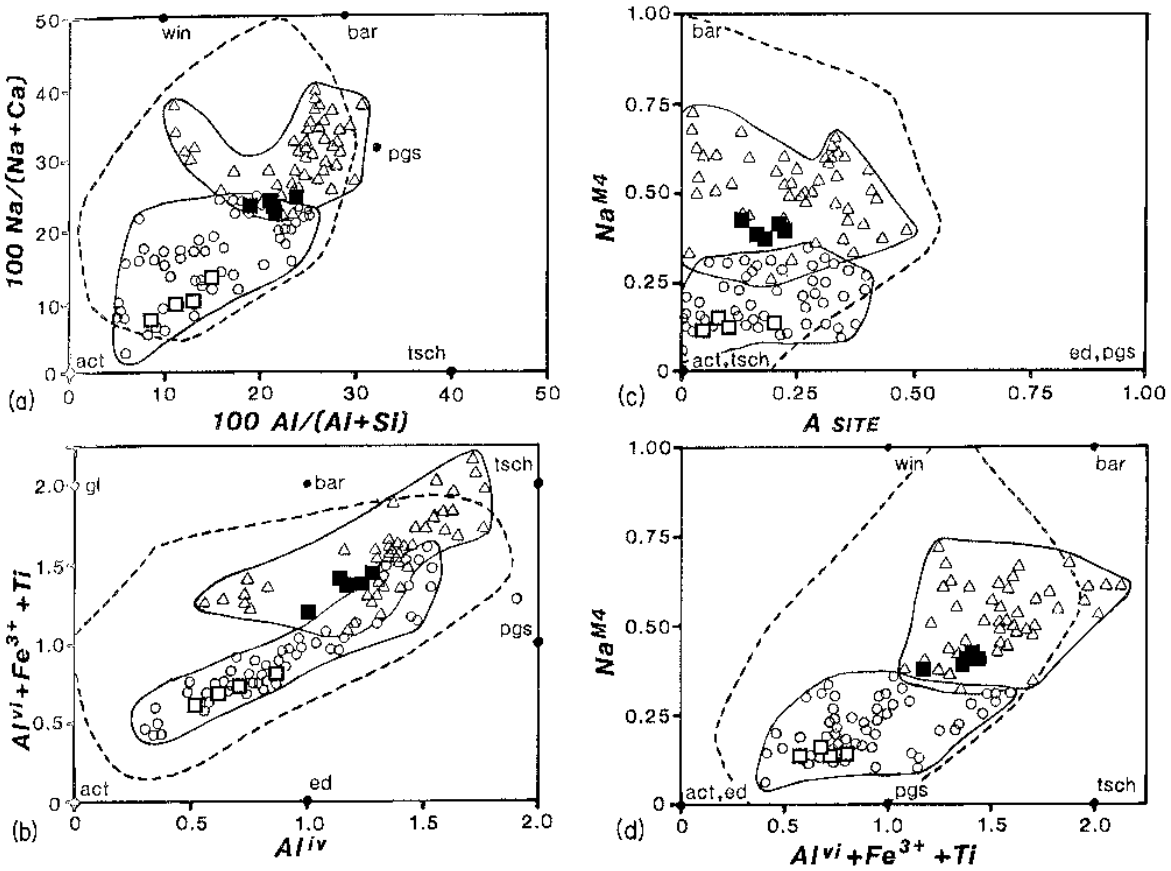

Fig. 5. TSZ amphibole composition in terms of substitutions used to discriminate tectonic environment as suggested by Laird & Albee (1981a, b). D_{Nds} (open triangles) and D_{Dss} (open circles) plot in separate fields; in all cases, D_{Dds} amphiboles show stronger glaucophane ($NaAl^{VI}Ca_{-1}Mg_{-1}$) substitution than D_{Dss}, indicating somewhat different metamorphic conditions. Both D_{Nds} and D_{Dss} amphiboles fall in the Sanbagawan and Fransican field of Laird & Albee (1981b) (dashed lines), which indicates that TSZ metamorphism is of a subduction zone environment. In (a) and (b), pressure increases along the *y*-axis and temperature along the *x*-axis. Closed squares are amphibole analyses from DW–280E; coarse-grained (filled) and fine-grained (open; locally as overgrowth rims) amphiboles plot within the D_{Nds} and D_{Dss} fields, respectively.

in chemical equilibrium. For reasons outlined below, the assumption of chemical equilibrium may not be valid across the entire microprobe section. Each composition used for thermobarometric calculations consists of an average of 2–6 adjacent spot analyses of each mineral. *P–T* calculations for each mineral pair or suite are represented graphically; K_{eq} lines were plotted with the computer programs of Spear (1990). Compositions of representative mineral pairs or suites for each sample are presented in Tables 3–7.

Calcite–dolomite thermometry

Mg is partitioned between coexisting calcite and dolomite as a funtion of temperature (Graf & Goldsmith, 1955; Goldsmith & Heard, 1961). Although the solvus is well calibrated between 400 and 800° C (Goldsmith & Newton, 1969; Anovitz & Essene, 1982; Powell *et al.*, 1984), application of this thermometer may be problematic due to retrogressive exsolution (Essene, 1982). In order to minimize the effect of retrogression, a broad electron beam was used during microprobe analysis, and several spots were averaged to estimate grain composition at peak metamorphic conditions (Perkins *et al.*, 1982).

Two D_{Rds} and three $D_{Dssd'A}$ carbonate tectonites contain coexisting calcite and dolomite (Fig. 6). Analyses are precise to ±5% error in $X_{Mg,cc}$ and $X_{Fe,dol}$. D_{Rds} tectonites yield temperatures of 360–420° C; the presence of actinolite, albite, epidote and chlorite in D_{Rds} metabasalt requires pressures greater than 2–3 kbar (Maruyama *et al.*, 1983). Several samples which contain $D_{Dssd'A}$ tectonite fabrics yield temperatures of 390–515° C. The difference in temperatures obtained from the D_{Rds} and $D_{Dssd'A}$ carbonates is probably significant, and suggests that either D_{Rds} deformation occurred at lower temperature than $D_{Dssd'A}$, or D_{Rds} peak temperature was lower in the north,

Table 1. Representative amphibole compositions for DW-280E.

Sample	2c2	2c3	3c5	2f1	2f2	4f3
	coarse-grained			fine-grained		
SiO_2	48.01	46.27	47.02	52.70	51.41	50.90
TiO_2	0.30	0.36	0.33	0.12	0.13	0.08
Al_2O_3	11.00	12.19	11.81	4.41	6.36	5.46
FeO	13.69	13.80	13.50	11.15	11.24	13.05
MnO	12.20	0.24	0.28	0.35	0.36	14.15
MgO	0.29	11.47	11.81	16.22	15.32	0.29
CaO	10.31	10.33	10.36	12.43	12.30	11.93
Na_2O	1.76	1.89	1.99	0.49	0.72	0.69
K_2O	0.37	0.46	0.36	0.12	0.16	0.17
Total	97.21	97.35	97.77	97.46	98.59	97.12
	normalized to 23 oxygens					
Si	6.852	6.701	6.765	7.464	7.298	7.380
Al^{iv}	1.148	1.299	1.235	0.536	0.702	0.620
Al^{vi}	0.703	0.782	0.768	0.200	0.362	0.313
Ti	0.032	0.039	0.036	0.013	0.014	0.009
Cr	0.000	0.001	0.005	0.000	0.004	0.001
Fe^{3+}	0.673	0.615	0.575	0.382	0.339	0.355
Mg	2.596	2.477	2.533	3.425	3.242	3.059
Fe^{2+}	0.951	1.056	1.049	0.939	0.995	1.227
Mn	0.035	0.029	0.034	0.042	0.043	0.036
Ca	1.577	1.603	1.597	1.886	1.781	1.853
Na(M4)	0.432	0.397	0.403	0.114	0.129	0.147
Na(A)	0.064	0.134	0.152	0.021	0.069	0.047
K	0.067	0.085	0.066	0.022	0.029	0.031
Total	15.131	15.219	15.218	15.042	15.098	15.079
$Fe^{2+}/(Fe^{2+}+Mg)$	0.270	0.299	0.293	0.215	0.235	0.286
$Fe^{3+}/(Fe^{3+}+Al^{vi})$	0.489	0.440	0.428	0.656	0.484	0.531

as recorded by LP-51A and LP-52A, and higher to the south (DC-125, DC-129, and LV-223C). Also, it is possible that LV-223C records deformation and metamorphism associated with D_{Dss}. Sample LV-233C contains two different occurrences of carbonate. Calcite–dolomite pairs within the foliation give temperatures of 395–515° C, whereas mineral pairs in veins perpendicular to Le_{ss} yield temperatures of 340–365° C. Vein temperatures are interpreted to reflect the waning stages of ductile deformation (presumably dextral shear along the d'Abbadie fault), whereas the higher temperatures obtained from calcite–dolomite pairs within the foliation reflect earlier, higher grade conditions.

Garnet–mica schist thermobarometry

A number of exchange thermobarometric calibrations exist for garnet–mica schist. Garnet–biotite and garnet–biotite–muscovite–plagioclase exchange thermobarometers were used, and the garnet–biotite–plagioclase barometer (Hoisch, 1990) was used in one sample in which white mica was not in close proximity to the other mineral phases.

Fe–Mg exchange between coexisting garnet and biotite has been calibrated as a thermometer by many workers (Thompson, 1976; Goldman & Albee, 1977; Ferry & Spear, 1978; Ganguly, 1979; Hodges & Spear, 1982). Garnet–biotite pairs from nine D_{Nds}, three D_{Dss} and three Cassiar tectonites were analysed. As garnet in TSZ and Cassiar tectonites is relatively rich in grossular component (Table 4), Hodges & Spear's (1982) calibration was used. Mineral pairs are limited to garnet with $X_{Mn} < 0.25$, and biotite with $X_{Al} < 0.20$ and $X_{Ti} < 0.05$ in the octahedral site. All TSZ garnet core–biotite matrix pairs give temperatures *c.* 50° C lower than garnet rim–biotite rim pairs. Rim–rim pairs are used throughout this study, unless otherwise noted. Estimated errors are ±50° C (Hodges & Spear, 1982).

Garnet–biotite–muscovite–plagioclase thermobarometry, which considers changes in Al and Mg–Fe coordination in muscovite and plagioclase as a function of pressure, and Mg–Fe exchange in garnet–biotite as a function of temperature, has been empirically calibrated and shown to be useful for metasedimentary rocks which lack aluminium silicate phases (Ghent & Stout, 1981). Recalibration of this thermobarometer with regard to grossular component (Hodges & Crowley, 1985) is used to determine P–T conditions in four D_{Nds}, one D_{Dss} and two Cassiar tectonites. The samples contain K-feldspar; X_{an} is ≥0.12 in plagioclase. Pressures determined by this method are probably minima, as in each case the highest X_{an} value (generally $X_{an} \geq 0.20$) was used. Tectonites from the southern part of the area with the appropriate mineral assemblage have plagioclase with $X_{an} = 0.005$–0.05; these were not used. Mixing models used to calculate An activity (Orville, 1972) break down, due to the peristerite solvus, if X_{an} is ≤0.07 (Ghent & Stout, 1981). Ashworth & Evirgen (1985) caution against using this thermobarometer if X_{an} is ≤0.20. Errors of ±50° C and ±1–1.5 kbar are estimated for the calibration (Hodges & Crowley, 1985).

In a few samples, garnet, biotite, muscovite and plagioclase are not in contact in portions of the probe section free of evident retrogression. In these cases the empirically calibrated garnet–biotite–plagioclase barometer of Hoisch (1990) was used, which was derived with similar compositional constraints.

The results of thermobarometric analysis are plotted for each of three TSZ subareas and for Cassiar tectonites (Fig. 7). Garnet–biotite temperatures range from 400 to 750° C; D_{Nds} temperatures are from 550 to 750° C. Along strike, average temperatures from D_{Nds} tectonites in the southern subarea (Fig. 7a) are lower than the average temperatures recorded in the central and northern subareas (Fig. 7b, c). Some D_{Nds} tectonites yield temperatures from different mineral pairs that are within the precision of the calibration (e.g. LV-184 & LV-197AB), whereas others yield a range of temperatures (e.g. DW-321 & DW-325). DW-291 records a pressure of *c.* 17 kbar, although plagioclase in this sample is Ab-rich (X_{an} *c.* 0.13). Synkinematic pressures determined from two barometers range from 7 to 15 kbar in the northern and central subareas. No pressure calculations were possible for rocks in the southern area, although the presence of albite indicates a minimum pressure of *c.* 8 kbar (Fig. 7a).

One of the most striking aspects of these data is that the temperatures recorded by D_{Dss} tectonites are consistently

Table 2. Mineral assemblages of silicate rocks used for quantitative geothermobarometry.

Sample	Qtz	Kfs	Ab	Pl	Ms	Bt	Grt	Hbl	Ep	Chl	Ttn	Ap	Zrn	Mag	Rt	Ilm	GB	GP	GH	HP	WM	D_{Nds}	D_{Dss}	$D_{Dssd'A}$	Cas
LV-184	X		X		X	X	X	X	X	X	X			X			✓		✓			Δ			
LV-189	X		X		X	X	X	X	X	X	X		X	X			✓					Δ			
LV-192A	X		X		X		X	X	X	X	X			X	X				✓			Δ			
LV-193F	X		X		X		X	X	X	X	X			X	X				✓			Δ			
LV-197AB	X		X		X	X	X	X	X	X	X			X			✓					Δ			
TW-242C	X	X		X	X	X				X						X					✓	Δ			
TW-245	X			X		X	X	X	X	X	X			X			✓					Δ			
TW-261	X		X		X	X	X	X		X		X	X	X	X	X	✓					Δ			
TW-263	X		X	X		X	X	X	X	X	X			X		X			✓	✓		Δ			
TW-263D	X		X	X	X	X	X			X		X	X	X	X	X	✓	✓				Δ			
DW-286	X	X	X		X	X			X							X					✓	Δ			
DW-288	X	X	X		X	X			X		X					X					✓	Δ			
DW-290	X	X	X	X	X	X	X	X	X	X	X	X		X					✓	✓		Δ			
DW-291	X	X	X		X	X	X		X	X	X	X	X	X			✓	✓				Δ			
DW-294	X		X			X	X	X	X	X	X	X	X	X					✓	✓		Δ			
DW-296	X			X	X	X	X	X	X	X				X	X	X			✓	✓		Λ			
DW-321	X	X	X		X	X	X	X		X		X		X	X	X	✓	✓				Δ			
DW-324	X		X			X	X	X	X	X				X	X	X	✓					Δ			
DW-325	X		X	X	X	X	X								X	X	✓	✓				Δ			
DW-280E	X	X	X		X	X			X	X		X				X					✓		Δ		
DW-282	X		X		X	X	X		X	X						X	✓						Δ		
DW-315B	X	X	X	X	X	X	X		X							X	✓	✓					Δ		
DW-315D	X		X	X	X	X	X	X	X	X		X				X	✓						Δ		
DC-109B	X	X		X	X	X				X		X	X			X					✓			Δ	
DC-111B	X	X		X	X	X					X		X			X					✓			Δ	
DC-112B	X	X		X	X	X						X				X					✓			Δ	
DE-330	X	X		X	X	X					X	X	X		X	X					✓				Δ
DE-332C	X	X		X	X	X	X					X	X	X	X	X	✓	✓							Δ
DE-339	X	X		X	X	X			X		X	X	X			X					✓				Δ
DE-345	X	X		X	X	X							X			X					✓				Δ
DE-347	X	X		X	X	X	X					X	X				✓	✓							Δ
DE-353	X	X		X	X	X			X			X	X	X	X	X					✓				Δ
DE-365C	X	X		X	X	X						X	X		X	X					✓				Δ
DE-370	X	X		X	X	X	X				X	X	X	X		X	✓	✓							Δ
DE-391	X	X		X	X	X			X			X	X			X					✓				Δ

GB = garnet–biotite thermometry; GP = garnet–biotite–muscovite–plagioclase thermobarometry; GH = garnet–hornblende thermometry; HP = garnet–hornblende–plagioclase barometry; WM = white mica barometry; D_{Nds}, D_{Dss}, $D_{Dssd'A}$ and Cas are tectonite domains discussed in the text.

lower than the temperatures recorded by nearby D_{Nds} tectonites (Fig. 7b), as is shown also by the amphibole data discussed above. Sample DW-321 is structurally transitional between D_{Nds} and D_{Dss} and it shows *P–T* values consistent with both D_{Nds} and D_{Dss} deformation. D_{Dss} tectonite DW-315B also yields a range in *P–T* as determined from ten garnet–biotite pairs and six mineral suites.

Many samples yield a range in *P–T* conditions (such as DW-315B & DW-321; Fig. 7b). The variation in calculated *P–T* may result from chemical disequilibrium, or it may reflect persistence of local equilibrium due to heterogeneous strain and strain partitioning at the grain scale, reflecting real changes in *P–T* conditions during progressive ductile deformation. I interpret the range in *P–T* recorded within these samples to reflect changes in *P–T* conditions which accompanied ductile deformation. This interpretation is supported by amphiboles from D_{Dss} tectonite DE-280, which are zoned with barroisite-rich cores and actinolite-rich rims.

The three Cassiar tectonites exhibit a broad range of temperature and pressure (*c.* 525–750° C and 7–13 kbar) (Fig. 7d). Coexisting garnet–biotite–plagioclase from tectonite DE-347 record significantly lower *P–T*, as calculated from garnet and plagioclase cores with matrix biotite, than *P–T* calculated using garnet and plagioclase rims. Core–rim relations record prograde (i.e. positive $\Delta P/\Delta T$) dynamothermal metamorphism. Tectonite DE-332C shows a similar prograde trend as calculated from garnet core to rim, using matrix plagioclase and biotite.

Amphibolite thermobarometry

Graham & Powell (1984) calibrated Fe–Mg partitioning between coexisting garnet and hornblende as a thermometer. Garnet–hornblende pairs from seven D_{Nds} tectonites were analysed (Tables 2, 3 & 7); no garnet–hornblende pairs were found in other structural domains. Kohn & Spear (1990) developed an empirically calibrated garnet–hornblende–plagioclase exchange barometer. Two TSZ tectonites (TW-263 & DW-290) have mineral assemblages and mineral compositions which are within the limits of this barometer.

Quantitative *P–T* constraints calculated from D_{Nds}

Table 3. Garnet compositions.

Sample	184.2	189.1	197.2	245.2	261.1	263D.6	282.3	291.2	315B.7	315D.2	321.2	324.1	325.1	332C.6	347.3	347.3	370.4
SiO_2	38.11	38.11	38.73	38.92	38.91	38.01	37.83	38.65	38.04	38.49	38.93	38.57	38.65	38.53	38.84*	38.92†	38.44
TiO_2	0.05	0.07	0.14	0.07	0.07	0.05	0.12	0.09	0.10	0.15	0.09	0.12	0.10	0.05	0.14	0.03	0.05
Al_2O_3	21.78	21.48	21.80	21.45	21.89	21.64	21.43	21.90	21.32	21.39	21.75	21.95	21.93	21.73	21.73	21.90	21.79
FeO	23.49	24.81	22.85	20.06	28.57	32.85	25.61	24.22	27.24	26.77	24.95	27.88	28.06	31.15	27.46	28.90	31.06
MnO	6.86	4.35	0.27	4.74	3.52	1.46	8.57	0.77	4.81	4.21	0.38	5.36	0.67	0.75	2.07	0.39	0.26
MgO	1.75	1.85	1.31	1.52	3.16	2.87	1.73	2.16	1.13	1.38	3.11	3.48	2.76	2.33	1.17	1.80	2.48
CaO	9.38	9.85	16.46	14.88	6.27	4.98	6.30	12.97	8.70	9.16	11.69	4.69	8.99	7.13	10.83	9.81	8.06
Total	101.44	100.52	101.57	101.63	102.39	101.86	101.60	100.83	101.34	101.56	100.91	102.10	101.15	101.70	102.29	101.78	102.17
								normalized to 12 oxygens									
Si	2.989	3.007	2.996	3.014	3.013	2.987	2.991	3.007	3.007	3.021	3.017	3.000	3.011	3.014	3.018	3.026	2.994
Ti	0.003	0.004	0.008	0.004	0.004	0.003	0.007	0.005	0.006	0.009	0.005	0.007	0.006	0.003	0.008	0.002	0.003
Al	2.014	1.998	1.988	1.958	1.998	2.005	1.997	2.009	1.987	1.979	1.987	2.013	2.014	2.004	1.990	2.007	2.001
Fe^{2+}	1.541	1.637	1.478	1.299	1.850	2.159	1.693	1.576	1.801	1.757	1.617	1.814	1.828	2.038	1.784	1.879	2.023
Mn	0.456	0.291	0.018	0.311	0.231	0.097	0.574	0.051	0.322	0.280	0.025	0.353	0.044	0.050	0.136	0.026	0.017
Mg	0.204	0.218	0.151	0.175	0.365	0.336	0.204	0.250	0.133	0.162	0.359	0.403	0.320	0.272	0.136	0.209	0.288
Ca	0.788	0.833	1.364	1.235	0.520	0.419	0.534	1.081	0.737	0.770	0.971	0.391	0.750	0.598	0.902	0.817	0.673
Fe/(Fe + Mg)	0.883	0.882	0.907	0.881	0.835	0.865	0.892	0.863	0.931	0.916	0.818	0.818	0.851	0.882	0.929	0.900	0.875
Pyrope	0.068	0.073	0.050	0.058	0.123	0.112	0.068	0.085	0.044	0.055	0.121	0.136	0.109	0.092	0.046	0.071	0.096
Alman	0.516	0.550	0.491	0.430	0.624	0.717	0.563	0.533	0.602	0.592	0.544	0.613	0.621	0.689	0.603	0.641	0.674
Spess	0.153	0.098	0.006	0.103	0.078	0.032	0.191	0.017	0.108	0.094	0.008	0.119	0.015	0.017	0.046	0.009	0.006
Gross	0.264	0.280	0.453	0.409	0.175	0.139	0.178	0.365	0.246	0.259	0.327	0.132	0.255	0.202	0.305	0.279	0.224

Sample	184.5	192A.5	193F.2	263.1	290.1	294.1	296A.4
SiO_2	38.21	38.42	38.60	37.89	38.55	38.52	38.75
TiO_2	0.12	0.20	0.12	0.12	0.10	0.15	0.07
Al_2O_3	21.33	21.64	21.62	21.31	21.56	21.95	21.73
FeO	30.30	25.97	26.52	31.40	21.45	25.76	29.36
MnO	0.88	2.72	0.67	1.15	1.72	2.71	0.63
MgO	2.63	3.07	2.67	1.75	2.16	2.48	4.76
CaO	7.54	9.13	10.88	7.61	15.18	10.32	6.16
Total	101.04	101.20	101.20	101.25	100.75	101.92	101.48
Si	3.008	2.997	3.006	2.998	2.998	2.988	3.003
Ti	0.007	0.012	0.007	0.007	0.006	0.009	0.004
Al	1.980	1.990	1.985	1.988	1.977	2.007	1.985
Fe^{2+}	1.995	1.694	1.727	2.078	1.395	1.671	1.903
Mn	0.059	0.180	0.044	0.077	0.113	0.178	0.041
Mg	0.308	0.357	0.310	0.206	0.250	0.287	0.549
Ca	0.636	0.763	0.908	0.645	1.265	0.858	0.511
Fe/(Fe + Mg)	0.866	0.826	0.848	0.910	0.848	0.853	0.776
Pyrope	0.103	0.119	0.104	0.069	0.083	0.096	0.183
Alman	0.665	0.566	0.578	0.691	0.461	0.558	0.634
Spess	0.020	0.060	0.015	0.026	0.037	0.059	0.014
Gross	0.212	0.255	0.304	0.215	0.418	0.287	0.170

* core, † rim.

Table 4. Biotite compositions.

Sample	184.2	189.1	197.2	245.2	261.1	263D.b2	282.3	291.2	315B.4	315D.2	321.2	324.1	325.1	332C.6	347.3	370.4
SiO_2	36.65	36.56	37.07	37.37	36.16	35.42	37.96	38.50	35.33	37.55	37.10	37.99	36.92	36.60	36.61	34.97
TiO_2	1.26	0.55	0.12	1.45	1.31	1.54	1.55	2.05	2.07	1.75	1.26	1.42	1.83	1.11	1.96	2.72
Al_2O_3	17.27	17.43	18.52	18.42	19.03	18.65	16.04	17.48	17.16	16.22	17.49	17.12	18.63	19.60	18.17	19.52
FeO	19.10	18.40	19.22	17.25	17.44	20.23	18.37	18.10	22.01	16.73	15.52	16.81	18.15	20.21	20.77	23.98
MnO	0.47	0.31	0.28	0.32	0.42	0.14	0.52	0.27	0.24	0.42	0.12	0.33	0.08	0.09	0.26	0.14
MgO	10.87	11.19	11.21	11.66	11.26	9.96	10.21	9.33	8.33	12.69	12.57	12.93	10.60	8.97	8.58	7.31
CaO	0.07	0.05	0.05	0.10	0.04	0.00	0.09	0.07	0.01	0.05	0.06	0.03	0.02	0.04	0.01	0.04
Na_2O	0.01	0.00	0.00	0.02	0.04	0.01	0.00	0.01	0.11	0.07	0.12	0.12	0.09	0.01	0.06	0.05
K_2O	9.54	9.66	9.88	9.61	9.88	9.92	9.57	8.76	9.56	9.72	9.44	9.60	9.41	9.64	9.81	9.96
Total	95.24	94.16	96.36	96.20	95.59	95.87	94.31	94.61	94.82	95.20	93.69	96.34	95.72	96.33	96.27	96.76
								normalized to 11 oxygens								
Si	2.790	2.806	2.784	2.779	2.722	2.698	2.903	2.901	2.749	2.828	2.813	2.818	2.768	2.755	2.776	2.663
Ti	0.072	0.032	0.007	0.081	0.074	0.088	0.089	0.116	0.121	0.099	0.072	0.079	0.103	0.063	0.112	0.156
Al^{iv}	1.210	1.194	1.216	1.221	1.278	1.302	1.097	1.099	1.251	1.172	1.187	1.182	1.232	1.245	1.224	1.337
Al^{vi}	0.340	0.383	0.424	0.394	0.411	0.373	0.349	0.454	0.323	0.268	0.376	0.315	0.415	0.494	0.400	0.415
Fe^{2+}	1.216	1.181	1.207	1.073	1.098	1.289	1.175	1.141	1.432	1.054	0.984	1.043	1.138	1.272	1.317	1.400
Mn	0.030	0.020	0.018	0.020	0.027	0.009	0.034	0.017	0.016	0.027	0.008	0.021	0.005	0.006	0.017	0.009
Mg	1.233	1.280	1.255	1.292	1.263	1.131	1.164	1.048	0.966	1.425	1.420	1.429	1.184	1.006	0.970	0.829
Ca	0.006	0.004	0.004	0.008	0.003	0.000	0.007	0.006	0.001	0.004	0.005	0.002	0.002	0.003	0.001	0.003
Na	0.002	0.000	0.000	0.003	0.006	0.001	0.000	0.002	0.016	0.010	0.018	0.017	0.013	0.001	0.009	0.007
K	0.927	0.946	0.947	0.912	0.949	0.964	0.934	0.842	0.949	0.934	0.913	0.908	0.900	0.926	0.949	0.968
Fe/(Fe + Mg)	0.497	0.480	0.490	0.454	0.465	0.533	0.502	0.521	0.597	0.425	0.409	0.422	0.490	0.558	0.576	0.628

Table 5. White mica compositions.

Sample	263D.6	291.2	315B.7	321.2	325.1	332C.6	370.4
SiO_2	46.27	48.87	47.89	47.54	49.19	46.67	45.98
TiO_2	0.56	0.65	0.55	0.19	0.95	0.36	0.57
Al_2O_3	34.31	28.45	28.54	29.37	31.14	34.56	34.42
FeO	2.11	3.04	4.43	3.22	2.51	1.27	1.66
MnO	0.02	0.05	0.05	0.02	0.04	0.00	0.04
MgO	0.89	2.46	2.19	1.98	2.54	1.00	0.85
CaO	0.01	0.00	0.01	0.04	0.01	0.04	0.01
Na_2O	0.88	0.23	0.47	0.26	0.40	0.29	0.35
K_2O	10.25	11.03	10.38	10.97	9.06	10.62	11.00
Total	95.34	94.78	94.54	93.62	95.87	94.89	94.94
			normalized to 11 oxygens				
Si	3.093	3.307	3.268	3.262	3.240	3.116	3.088
Ti	0.028	0.033	0.028	0.010	0.047	0.018	0.029
Al^{iv}	0.907	0.693	0.732	0.738	0.760	0.884	0.912
Al^{vi}	1.797	1.577	1.564	1.638	1.658	1.836	1.813
Fe^{2+}	0.118	0.172	0.253	0.185	0.138	0.071	0.093
Mn	0.001	0.003	0.003	0.001	0.002	0.000	0.002
Mg	0.089	0.248	0.223	0.202	0.249	0.100	0.085
Ca	0.001	0.000	0.001	0.003	0.001	0.003	0.001
Na	0.114	0.030	0.062	0.035	0.051	0.038	0.046
K	0.874	0.952	0.904	0.960	0.761	0.905	0.942
Fe/(Fe + Mg)	0.570	0.410	0.532	0.478	0.357	0.415	0.522
X_{Ca}	0.001	0.000	0.001	0.003	0.001	0.003	0.001
X_{Na}	0.115	0.031	0.064	0.035	0.063	0.040	0.047
X_K	0.884	0.969	0.935	0.962	0.936	0.957	0.952

Table 7. Hornblende compositions.

Sample	184.5	192A.2	193F.2	263.2	290.1	294.1	296A.4
SiO_2	44.73	44.41	45.19	42.15	44.93	43.83	43.22
TiO_2	0.58	0.53	0.45	0.45	0.52	0.56	0.56
Al_2O_3	13.78	14.49	14.14	13.55	12.85	15.42	14.95
FeO	16.38	15.34	14.35	20.85	13.28	15.52	16.80
MnO	0.29	0.22	0.19	0.23	0.34	0.29	0.30
MgO	9.59	9.75	10.33	7.00	11.49	9.52	9.47
CaO	9.73	8.62	9.84	11.28	11.36	10.68	8.98
Na_2O	2.11	3.28	2.25	1.48	1.59	2.06	2.34
K_2O	0.67	0.55	0.56	0.76	1.07	0.68	0.48
Total	97.86	97.21	97.35	97.77	97.46	98.59	97.12
			normalized to 23 oxygens				
Si	6.486	6.455	6.545	6.333	6.564	6.342	6.265
Al^{iv}	1.514	1.545	1.455	1.667	1.436	1.658	1.735
Al^{vi}	0.841	0.937	0.959	0.732	0.776	0.972	0.819
Ti	0.063	0.058	0.049	0.051	0.057	0.061	0.061
Fe^{3+}	0.805	0.780	0.608	0.625	0.340	0.549	1.258
Fe^{2+}	1.182	1.085	1.130	1.995	2.502	1.329	0.779
Mn	0.036	0.027	0.023	0.029	1.282	0.036	0.037
Mg	2.073	2.113	2.230	1.568	0.042	2.054	2.046
Ca	1.512	1.342	1.527	1.816	1.778	1.656	1.395
Na(M4)	0.488	0.658	0.473	0.184	0.222	0.344	0.605
Na(A)	0.105	0.267	0.159	0.247	0.228	0.234	0.052
K	0.124	0.102	0.103	0.146	0.199	0.126	0.089
Total	15.229	15.369	15.262	15.393	15.428	15.359	15.141
$Fe^{2+}/(Fe^{2+} + Mg)$	0.363	0.339	0.336	0.560	0.339	0.393	0.276
$Fe^{3+}/(Fe^{3+} + Al^{vi})$	0.489	0.454	0.388	0.460	0.305	0.361	0.606

amphibolite tectonites are presented in Fig. 8. As with the garnet–biotite results, garnet rim–hornblende rim temperatures are *c.* 50° C higher than garnet core–hornblende matrix temperatures. Rim–rim temperatures, interpreted to represent equilibrium conditions, are used. Garnet–hornblende temperatures are consistent within a sample, as well as throughout the study area, ranging from 530 to 660° C. The D_{Nds} garnet–hornblende temperature is similar to the garnet–biotite temperature. One sample (LV-184) yields garnet–biotite and garnet–hornblende temperatures of 540–600° C (compare Figs 7a & 8a).

Metamorphic pressure derived from TSZ mafic gneisses range from 7 to 12 kbar. Plagioclase in garnet–hornblende amphibolite from the southern TSZ subarea is albitic (*c.* An_{0-5}), hence the garnet–hornblende–plagioclase baro-

Table 6. Plagioclase compositions.

Sample	261.1	263D.6	291.2	315B.7	321.2	325.1	332C.6	347.3 core	347.3 rim	370.4	263.2	290.1	294.1	296A.4
SiO_2	61.01	63.27	64.57	60.63	61.89	57.85	57.38	62.44	61.60	55.13	61.06	59.92	65.49	63.81
Al_2O_3	24.29	22.13	21.82	24.73	22.34	26.78	26.79	23.45	24.00	27.73	23.70	24.04	21.16	21.50
CaO	6.21	3.55	2.75	6.26	4.83	9.01	8.70	4.95	5.64	10.34	6.12	6.65	2.14	2.95
Na_2O	8.16	9.39	10.33	8.26	9.10	6.47	6.50	8.80	8.41	5.67	8.02	7.71	10.70	10.10
K_2O	0.09	0.16	0.20	0.07	0.09	0.07	0.12	0.41	0.28	0.12	0.09	0.35	0.12	0.05
Total	100.19	98.60	99.88	100.20	98.43	100.25	99.60	100.12	100.23	99.19	99.10	99.12	99.69	99.47
							normalized to 8 oxygens							
Si	2.712	2.830	2.854	2.695	2.789	2.584	2.580	2.767	2.734	2.504	2.736	2.700	2.891	2.842
Al	1.273	1.167	1.137	1.296	1.187	1.410	1.420	1.225	1.256	1.485	1.252	1.277	1.101	1.129
Ca	0.296	0.170	0.130	0.298	0.233	0.431	0.419	0.235	0.268	0.503	0.294	0.321	0.101	0.141
Na	0.703	0.814	0.885	0.712	0.795	0.560	0.567	0.756	0.724	0.499	0.697	0.674	0.916	0.872
K	0.005	0.009	0.011	0.004	0.005	0.004	0.007	0.023	0.016	0.007	0.005	0.020	0.007	0.003
Ca/(Ca + Na)	0.296	0.173	0.128	0.295	0.227	0.435	0.425	0.237	0.270	0.502	0.297	0.323	0.099	0.139
An	0.295	0.171	0.127	0.294	0.226	0.433	0.422	0.232	0.266	0.499	0.295	0.316	0.099	0.139
Ab	0.700	0.820	0.863	0.702	0.770	0.563	0.571	0.746	0.718	0.495	0.700	0.664	0.895	0.858
Or	0.005	0.009	0.011	0.004	0.005	0.004	0.007	0.023	0.016	0.007	0.005	0.020	0.007	0.003

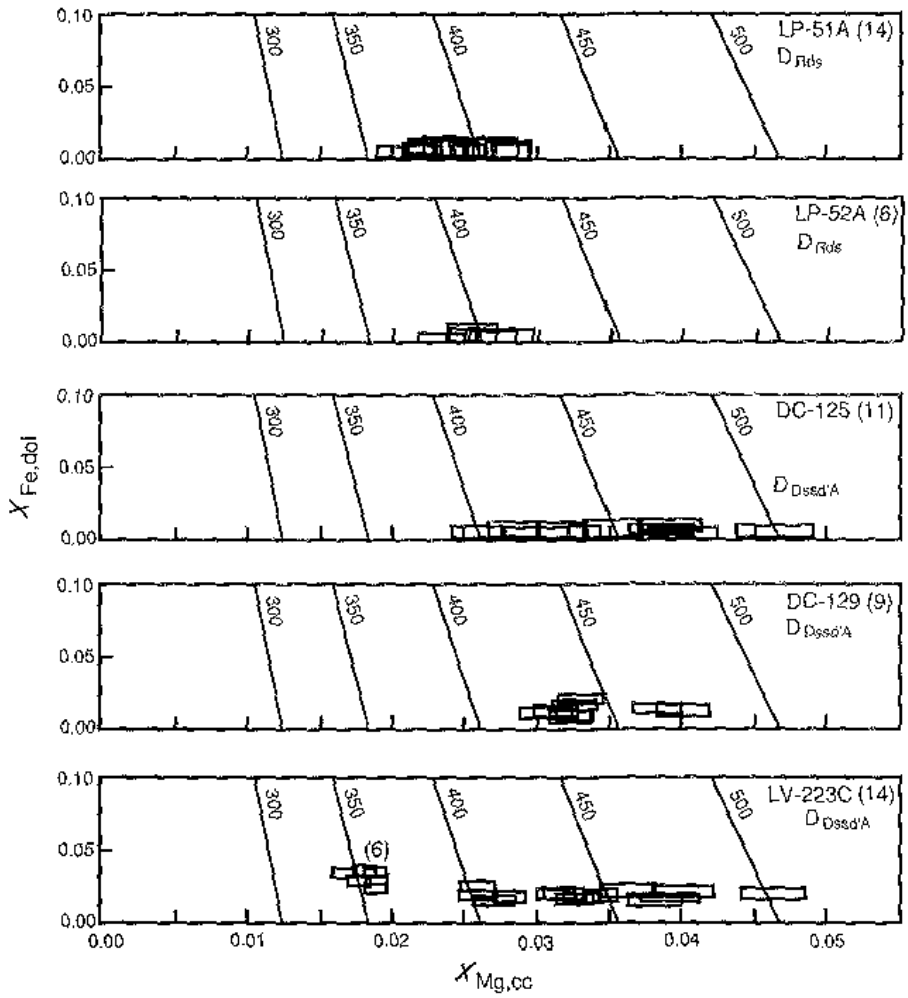

Fig. 6. A plot of $X_{Fe,dol}$ versus $X_{Mg,cc}$ for *two* D_{Nds} *and three* $D_{Dssd'A}$ *carbonate tectonites; boxes show compositional error* of ±5% and isotherms are in degrees centigrade. The number in parentheses indicates the number of coexisting calcite–dolomite pairs analysed. Fourteen coexisting mineral pairs within the foliation in LV-223C give temperatures which range from 385 to 515° C, whereas six mineral *pairs within fractures normal to Le give temperatures of* 340–365° C. *Calibration of* Powell *et al.* (1984).

meter is not applicable. However, a minimum pressure of 7–11 kbar can be estimated by taking the albite–oligoclase transition together with garnet–hornblende temperatures. Similarly, in the central region, DW-294 and DW-296 have albite-rich plagioclase ($X_{an} = 0.10$ and $X_{an} = 0.14$, respectively) that is outside the limits of the Kohn & Spear (1990) barometer ($X_{an} \geq 0.15$); however, the presence of albite with hornblende constrains minimum pressure for these samples to 10 kbar (at *c.* 625° C) and 12 kbar (at *c.* 675° C), respectively. DW-290 yields 650° C, 11 kbar from garnet–hornblende–plagioclase thermobarometry. In *the northern subarea, TW-263 yields c.* 8.5 kbar at *575–660° C; TW-263D, an immediately adjacent schist,* yields 9.5–11.5 kbar at 625–660° C from garnet–biotite–muscovite–plagioclase thermobarometry (Fig. 7c). *P–T* constraints derived from garnet–hornblende–plagioclase and garnet–biotite–muscovite–plagioclase thermobarometry are in good agreement. Albitic plagioclase was found in each of the samples; however, in each case the most anorthite-rich plagioclase close to the other minerals was analysed, and therefore pressure estimates are minima.

Fig. 7. *P–T* plots of garnet–mica schist thermobarometric constraints. Al_2SiO_5 phase boundaries (Holdaway, 1971) and the albite–oligoclase (ab–ol) transition for metabasalt (Maruyama *et al.*, 1983) are shown for reference. Each line or symbol represents one set of minerals; sets from the same sample are plotted with the same symbol. Steep lines represent Grt–Bt K_{eq}, short transverse lines mark Grt–Bt–Ms–Pl K_{eq}, or Grt–Bt–Pl K_{eq} (two intersecting lines). Symbols mark intersections for mineral suites. *P–T* conditions are higher for D_{Nds} tectonites than for D_{Dss} tectonites. Error bars shown in (c) are valid in (a), (b) and (d). (a) Grt–Bt calculations from the southern region: *LV-184* = dotted lines; *LV-189* = solid lines; and *LV-197AB* = dashed lines. (b) Grt–Bt and Grt–Bt–Ms–Pl calculations *from the central region:* D_{Nds} *samples show higher T and P than* D_{Dss} *samples.* D_{Nds} *samples: DW-321 (transitional between* D_{Nds} and D_{Dss}) = dotted lines, and filled rectangle; DW-324 = dashed lines; DW-325 = solid lines, and filled ellipse; DW-291 = dotted and dashed lines, and open diamonds. Pl is *c.* An_{9-10}. D_{Dss} samples: DW-282 = dashed lines; DW-315B = dotted lines, and open ellipses; DW-315D = solid lines. Note the wide range in conditions recorded by DW-315B. (c) Grt–Bt and Grt–Bt–Ms–Pl calculations from the northern region: TW-245 = solid lines; TW-261 = dashed lines, fitted ellipse = Grt–Bt–Pl; TW–263D = dotted lines, open ellipses = Grt–Bt–Ms–Pl. (d) Cassiar tectonites: DE-332C = dotted lines, and open rectangles = Grt–Bt–Ms–Pl or Grt–Bt–Pl; calculated temperature for two biotite inclusions in garnet is 560° C, consistent with prograde metamorphism indicated by core–rim relations. DE-347 = dashed lines, and open ellipses. Grey arrows show general prograde trend from core to rim for two mineral suites. *DE-370 = solid lines, and filled ellipses. Note the wide range in P–T conditions.*

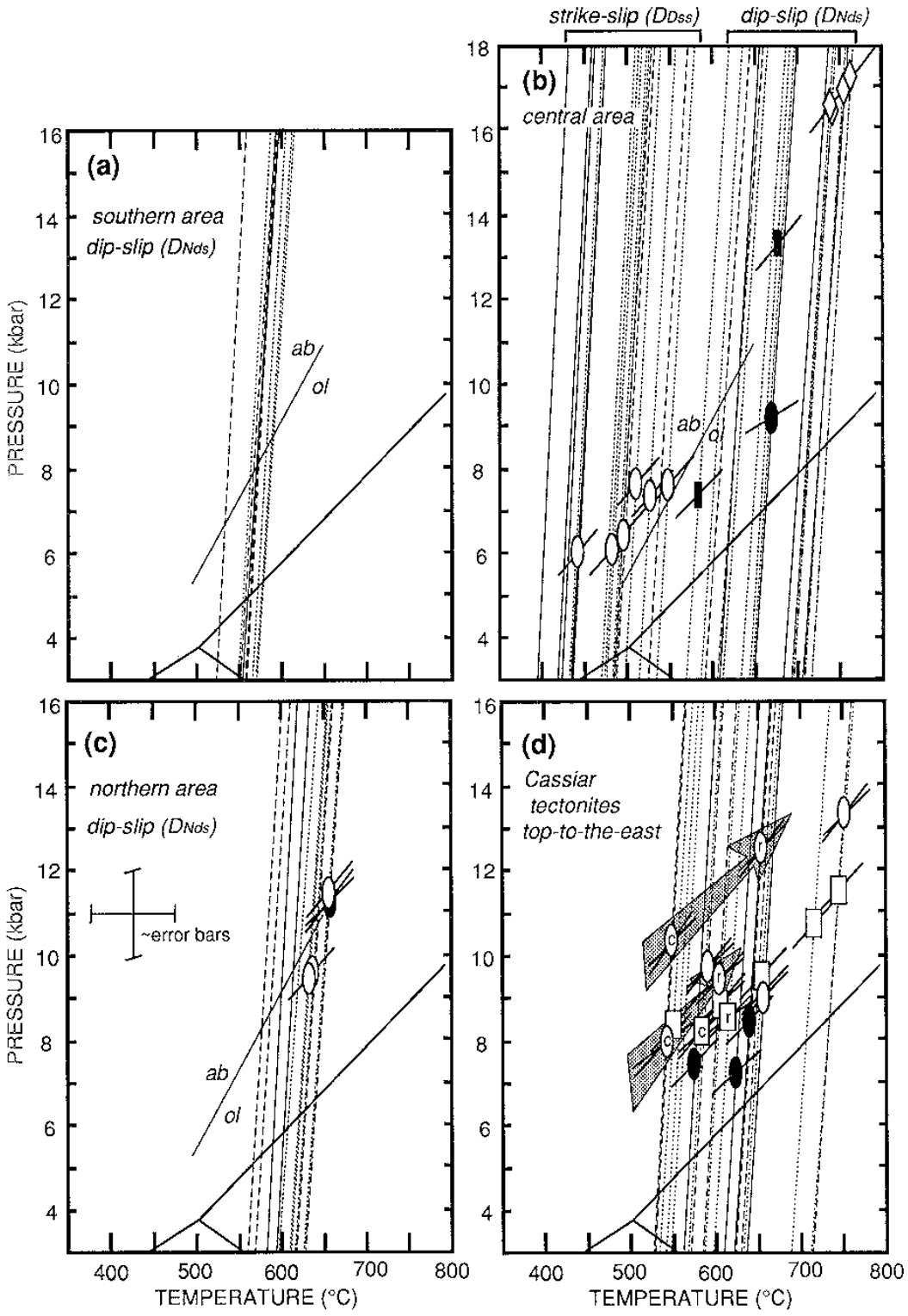
strike-slip (DDss)
dip-slip (DNds)
(a)
southern area
dip-slip (DNds)
(b)
central area
(c)
northern area
dip-slip (DNds)
~error bars
(d)
Cassiar
tectonites
top-to-the-east
ab
ol
PRESSURE (kbar)
TEMPERATURE (°C)
4
6
8
10
12
14
16
18
400
500
600
700
800

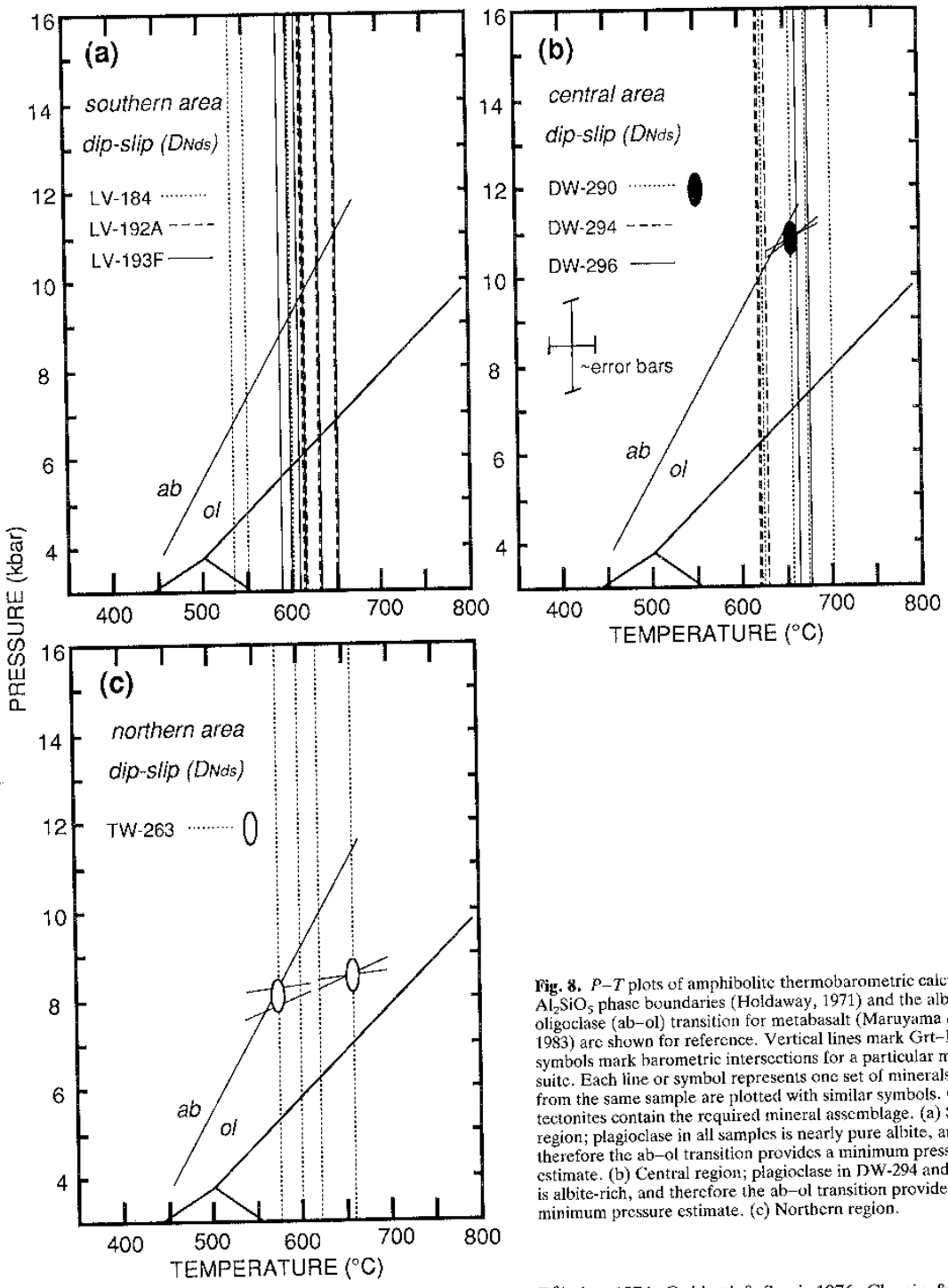

Fig. 8. *P–T* plots of amphibolite thermobarometric calculations. Al_2SiO_5 phase boundaries (Holdaway, 1971) and the albite–oligoclase (ab–ol) transition for metabasalt (Maruyama *et al.*, 1983) are shown for reference. Vertical lines mark Grt–Hbl K_{eq}, symbols mark barometric intersections for a particular mineral suite. Each line or symbol represents one set of minerals; sets from the same sample are plotted with similar symbols. Only D_{Nds} tectonites contain the required mineral assemblage. (a) Southern region; plagioclase in all samples is nearly pure albite, and therefore the ab–ol transition provides a minimum pressure estimate. (b) Central region; plagioclase in DW-294 and DW-296 is albite-rich, and therefore the ab–ol transition provides a minimum pressure estimate. (c) Northern region.

White mica barometry

White mica composition can be useful in identifying and constraining conditions of polymetamorphism (Boulter & Råheim, 1974; Guidotti & Sassi, 1976; Chopin & Maluski, 1980; Liewig *et al.*, 1981; Saliot & Velde, 1982; Frey *et al.*, 1983; Jacobson, 1984). The phengite component in white mica of a low-variance assemblage is an indication of the

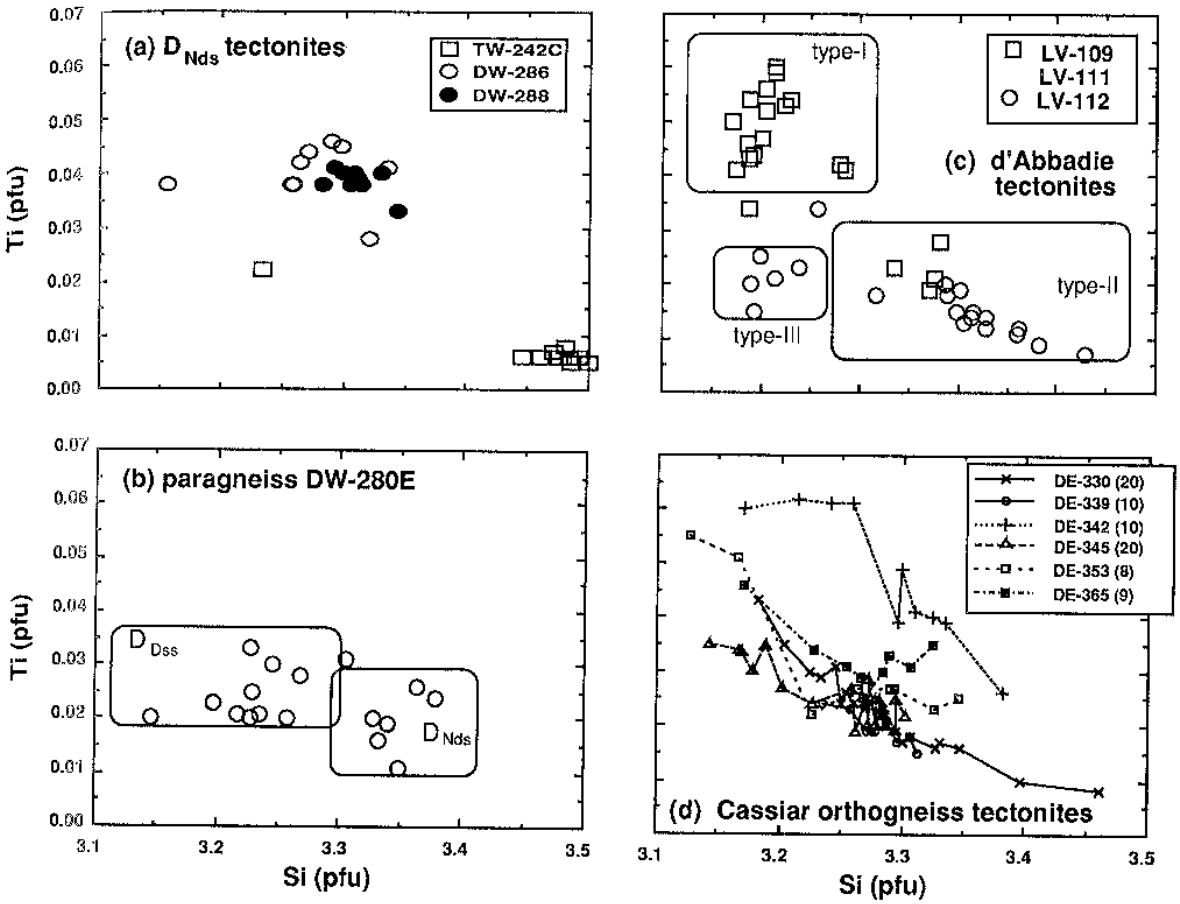

Fig. 9. White mica composition diagrams showing Si versus Ti content for micas from TSZ and Cassiar paragneisses and orthogneisses. Compositions normalized on the basis of 11 oxygens. (a) D_{Nds} tectonites: orthogneiss TW-242C, and paragneisses DW-286, DW-288. (b) D_{Dss} paragneiss DW-280E shows two populations of white mica composition, or a single population with gradational composition from high-Si to low-Si. (c) Orthogneisses DC-109, DC-111 and paragneiss DC-112 from the d'Abbadie shear zone have three white mica populations. Twenty grains from each sample. (d) White mica composition from six Cassiar orthogneisses. The number in parentheses indicates the number of grains from each sample.

pressure of its formation (Ernst, 1963; Velde, 1967; Guidotti & Sassi, 1976), and is calibrated by Massone & Schreyer (1987) as a barometer for Qtz + Bt + Wm + Kfs assemblages. The phengite, or tschermak, substitution, $(Fe^{2+}, Mg, Mn, Zn) + Si = (Al^{VI}, Fe^{3+}, Ti) + (Al^{IV})$, relates Ms-paragonite, $(K, Na)Al_2^{VI}(Si_3Al^{IV})O_{10}(OH)_2$, to celadonite, $K(R^{2+}R^{3+})Si_4O_{10}(OH)$. As in amphibole, the Ti content of biotite and white mica in a rock bearing a Ti-saturated phase qualitatively reflects the temperature of formation (Rasse, 1974; Ernst, 1988). Ti content in white mica increases with increasing temperature, and this relation may be used to discriminate igneous from metamorphic white mica. Phengite with Ti >0.04 per formula unit generally reflects an original igneous white mica, whereas those with <0.03 probably recrystallized during metamorphism. Thus, the Ti and Si content of white mica from the assemblage of Qtz + Bt + Wm + Kfs + Ti phase are useful in comparing qualitatively conditions of crystallization. Furthermore, pressure may be determined on the basis of the Si content in white mica, as a function of temperature, using isopleths of Massone & Schreyer (1987).

White mica was analysed from D_{Nds}, D_{Dss}, $D_{Dssd'A}$ and Cassiar tectonites. Each sample contains the limiting assemblage necessary for white mica barometry. Analyses of 9–20 grains (commonly preserved as fish) were obtained from each sample. Initially, core, intermediate and rim areas of each grain were analysed to check for zoning, but none was found. A minimum of two analyses, and generally three, was averaged to give a single grain composition. White mica in four TSZ tectonites was analysed, including one orthogneiss and two paragneisses from D_{Nds}, and one D_{Dss} paragneiss. Each sample is adjacent to one or more samples for which metamorphic temperature was determined.

White mica from D_{Nds} orthogneiss and paragneiss shows high Si, indicative of high-*P* metamorphism (Fig. 9a); Ti and Si values indicate that the white mica is probably of

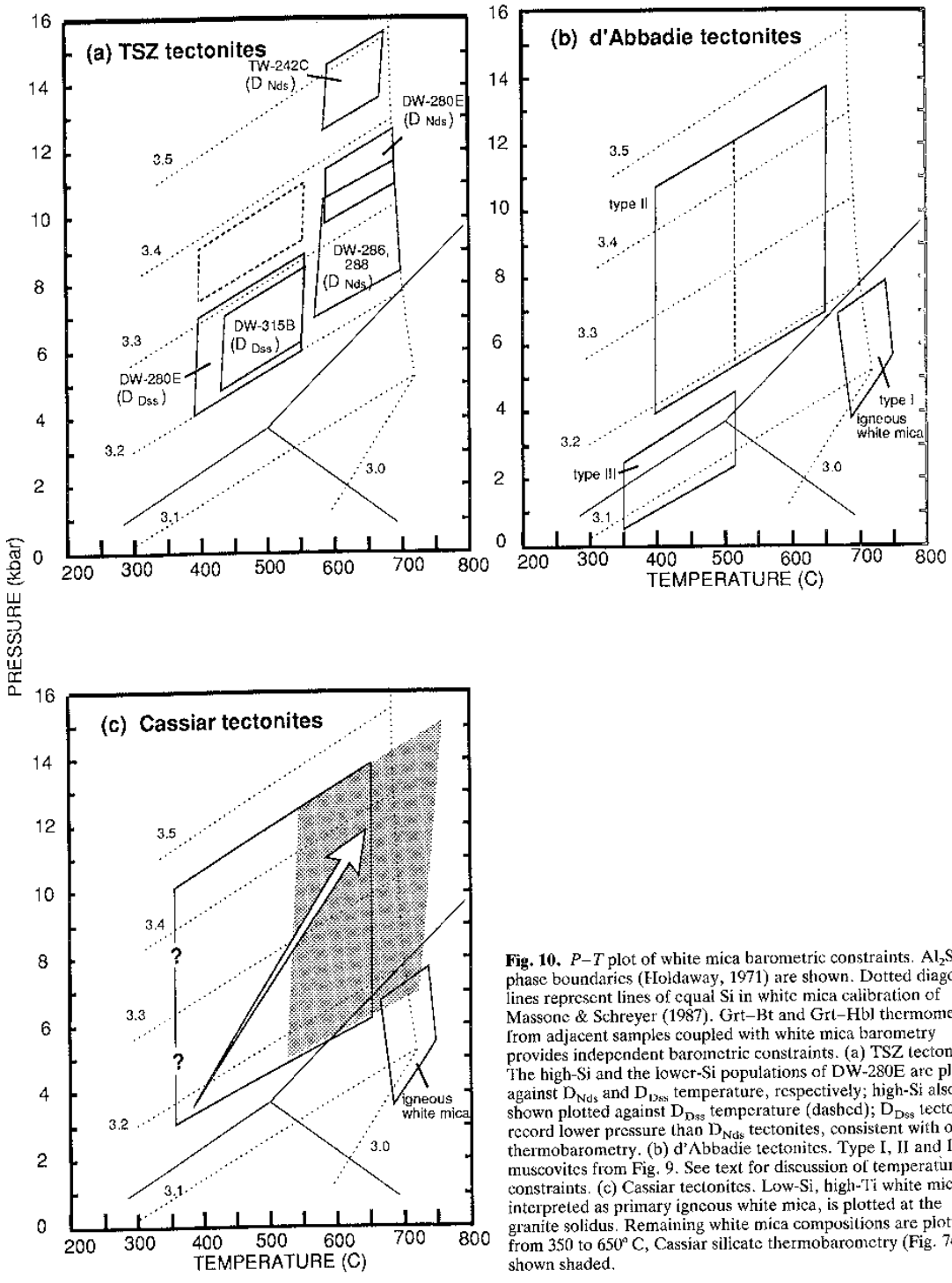

Fig. 10. *P–T* plot of white mica barometric constraints. Al_2SiO_5 phase boundaries (Holdaway, 1971) are shown. Dotted diagonal lines represent lines of equal Si in white mica calibration of Massone & Schreyer (1987). Grt–Bt and Grt–Hbl thermometry from adjacent samples coupled with white mica barometry provides independent barometric constraints. (a) TSZ tectonites. The high-Si and the lower-Si populations of DW-280E are plotted against D_{Nds} and D_{Dss} temperature, respectively; high-Si also shown plotted against D_{Dss} temperature (dashed); D_{Dss} tectonites record lower pressure than D_{Nds} tectonites, consistent with other thermobarometry. (b) d'Abbadie tectonites. Type I, II and III muscovites from Fig. 9. See text for discussion of temperature constraints. (c) Cassiar tectonites. Low-Si, high-Ti white mica, interpreted as primary igneous white mica, is plotted at the granite solidus. Remaining white mica compositions are plotted from 350 to 650° C, Cassiar silicate thermobarometry (Fig. 7d) shown shaded.

metamorphic origin. The Si content of white mica from orthogneiss and paragneiss plotted against D_{Nds} temperatures determined from silicate thermometry constrains pressure of formation to *c.* 14 ± 2 kbar and 10 ± 2 kbar, respectively (Fig. 10a).

Twenty white mica grains were analysed from DW-280E, a D_{Dss} paragneiss. The data show two compositionally distinct groups distinguished on the basis of Ti and Si (Table 8, Fig. 9b). No textural differences between the two groups were recognized. Both groups are low in Ti, although they have variable Si, indicative of a moderately high-*P* metamorphic white mica. One group, with Si between 3.3 and 3.4 per formula unit (pfu), probably formed at higher pressure than other micas with Si = 3.1–3.3 pfu. Although this tectonite is from the D_{Dss} shear zone that crosses the D_{Nds} domain, it presumably experienced penetrative D_{Nds} metamorphic conditions. Therefore, the high-Si micas may reflect the high pressure consistent with D_{Nds} dynamothermal conditions and the low-Si group may correlate with D_{Dss} conditions. On this basis, the ranges of Si of the high- and low-Si populations and the temperatures calculated from adjacent D_{Nds} and D_{Dss} tectonites are used, respectively, to estimate pressure (Fig. 10a). This procedure results in pressures of 7.5–14 kbar for D_{Nds} and 5–9.5 kbar for D_{Dss}, similar to *P–T* constraints derived from garnet–biotite–muscovite–plagioclase thermobarometry. Plotting the high-Si white mica against D_{Dss} temperatures results in pressures of 8–11 kbar, higher than the 5–8 kbar range calculated from silicate barometry.

Analysis of white mica fish from $D_{Dssd'A}$ orthogneiss and paragneiss tectonites reveals three populations defined on the basis of Si and Ti (Fig. 9c). No textural criteria distinguish the groups. High-Ti, low-Si types (Type I) probably represent primary igneous muscovite; low-Ti, high-Si white mica (Type II) reflects high-*P* metamorphism, and low-Ti, low-Si varieties (Type III), observed only in DC-112, record relatively low-*P* metamorphism. The Si of each of these groups is plotted against an estimate of temperature of formation in Fig. 10(b). Temperature near the granite solidus was assumed for Type I mica, and results in a pressure of 5–7 kbar. Type II mica records a high pressure regardless of the temperature against which it is plotted. The highest Si values of Type II white mica result in a peak pressure of 10–12 kbar at 400–515° C ($D_{Dssd'A}$ calcite–dolomite thermometry), and pressure up to 14 kbar at 650° C (Cassiar peak temperature). Type III micas are plotted against calcite–dolomite temperatures (350–515° C) for $D_{Dssd'A}$ tectonites, and gives pressures of 1–4 kbar. Despite the wide range in the temperature estimated for each white mica population, significant differences in pressure result. These are interpreted to reflect real changes in pressure (although not necessarily absolute values) during the history of these tectonites.

White mica from six samples of Cassiar orthogneiss were analysed to constrain pressure during ductile shearing. Twenty white mica fish from DE-330 show a range in composition from high-Ti with low-Si to low-Ti with high-Si (Fig. 9d). In five other samples white mica shows a similar range. If each is interpreted to reflect chemical equilibrium, these data serve as a monitor of changes in pressure during progressive ductile shear (Guidotti & Sassi, 1976; Frey *et al.*, 1983). Each orthogneiss contains some high-Ti, low-Si white mica indicating primary igneous crystallization. The resultant pressures are comparable to values for Type I white mica from orthogneisses DC-109 and DC-111 in the d'Abbadie fault zone (Fig. 10b). I interpret these micas as having formed during primary crystallization at 340–360 Ma (U–Pb, zircon; Hansen *et al.*, 1989). Peak Si values of all six Cassiar orthogneisses are >3.3 pfu and are accompanied by a progressive decrease in Ti; three of the six orthogneisses record peak Si > 3.35 pfu; and DE-330 records a peak value of *c.* 3.4 pfu. These Si values indicate minimum peak metamorphic pressures of *c.* 6, 7 and 10 kbar, respectively, at a minimum temperature of 350° C. Maximum pressures range up to 14 kbar (Fig. 10c).

If the white mica composition in these six Cassiar orthogneisses, which range from high-Ti, low-Si gradationally through low-Ti, high-Si, results from ductile shearing during changing *P–T*, then three different paths could explain the data. Increase in pressure is required for each path. The orthogneiss could follow a path which increases pressure and decreases temperature from primary igneous crystallization during dynamic recrystallization; also, it could follow a path which statically increases pressure and then dynamically decreases *P–T*; or the orthogneiss could statically cool to lower *P–T* conditions, and later be sheared under increasing *P–T* conditions. The first path requires an increase in pressure and concurrent decrease in temperature, and hence it is not geologically likely. The second path is geologically reasonable. However, quartz grains in the orthogneisses exhibit flat-field extinction and straight boundaries, in contrast to expected undulatory extinction and ragged boundaries if cooling accompanied deformation. The third prograde path is similarly geologically reasonable, and it is consistent with independent prograde core–rim trends documented in DE-332C and DE-347 (Fig. 7d). In addition, one might expect flat-field extinction quartz in a rock which experienced such a history. Final exhumation of the orthogneiss may not have been accompanied by ductile accommodation of crustal extension and tectonic unloading, because no low-Si and low-Ti white-mica composition is observed in any of the samples. Thus, all six Cassiar orthogneisses exhibit a record of white mica transitional between two end-member compositions. These compositions are consistent with a sequence of events including primary igneous crystallization (high-Ti, low-Si), followed by static cooling, later dynamothermal recrystallization under increasingly high *P–T* conditions (low-Ti, high-Si), and finally static exhumation and cooling. This interpretation is consistent with slow cooling, interpreted as resulting solely from erosion, as indicated by the $^{40}Ar/^{39}Ar$ cooling history of these tectonites (Hansen *et al.*, 1991).

If the white mica compositional variations in TSZ and Cassiar tectonites cannot be attributed to interference

Table 8. Representative white mica compositions from DW-280E.

	1MU1	2MU5	7MU6	2MU3	3MU7	1MU2
SiO_2	46.61	47.30	46.04	49.10	48.36	48.55
TiO_2	0.38	0.39	0.44	0.50	0.46	0.37
Al_2O_3	28.45	28.36	29.10	26.31	25.33	26.87
FeO	4.71	4.34	4.89	4.21	4.30	4.28
MnO	0.05	0.07	0.05	0.05	0.08	0.02
MgO	2.34	2.17	1.78	2.79	2.94	2.58
CaO	0.00	0.04	0.01	0.00	0.00	0.01
Na_2O	0.24	0.20	0.20	0.16	0.13	0.17
K_2O	11.05	11.25	11.14	11.26	11.09	11.11
Total	93.85	94.14	93.68	94.39	92.70	93.97
			normalized to 11 oxygens			
Si	3.227	3.258	3.198	3.364	3.378	3.340
Al^{iv}	0.773	0.742	0.802	0.636	0.622	0.660
Al^{vi}	1.549	1.561	1.581	1.489	1.464	1.519
Ti	0.020	0.020	0.023	0.026	0.024	0.019
Fe^{2+}	0.273	0.250	0.284	0.241	0.251	0.246
Mn	0.003	0.004	0.003	0.003	0.005	0.001
Mg	0.241	0.223	0.184	0.285	0.306	0.265
Ca	0.000	0.003	0.001	0.000	0.000	0.001
Na	0.032	0.027	0.027	0.021	0.017	0.023
K	0.976	0.989	0.987	0.984	0.988	0.975
Fe/(Fe + Mg)	0.531	0.529	0.607	0.458	0.451	0.481
X_{Ca}	0.000	0.003	0.001	0.000	0.000	0.001
X_{Na}	0.032	0.026	0.027	0.021	0.017	0.023
X_K	0.968	0.971	0.972	0.979	0.983	0.976

from other phases, then the variable, and in some cases bimodal, white mica compositions may provide important clues to their dynamothermal evolution. Compositionally different generations of white mica may be preserved in these L-S tectonites as a result of addition of mechanical energy due to heterogeneous strain partitioning at the scale of a thin section. For example, it can be assumed that all white mica in orthogneisses DC-109 and DC-111 crystallized with a uniform mineral chemistry. Following crystallization, the granitoids acquired S-C fabrics. During deformation, it is possible that mica grains in certain domains were greatly strained, such as along C, whereas others were either protected from strain by more rigid minerals, or were located within areas of lower strain, such as within S (e.g. Bell & Hammond, 1984; Bell, 1985). Mica grains not protected from deformation would have undergone dynamic recrystallization, and their resultant chemical composition should reflect the ambient P–T conditions. Thus, some white mica may have recrystallized during early high-P ductile deformation and was either protected or re-equilibrated during later deformation; mechanical strain energy may therefore have exceeded the activation energy necessary to achieve chemical equilibrium within a new physical environment. This process may be particularly important when ductile deformation is near the temperature of recrystallization.

Tectonites DW-280E, DC-109, DC-111 and DC-112 contain evidence to suggest that they experienced at least two episodes of ductile deformation. DW-280E white mica data are consistent with field, structural and kinematic relations which suggest that this tectonite experienced early high-P/T dip-slip shear followed by strike-slip shear at lower (although also moderately high-P) P–T conditions. All penetrative deformation occurred prior to cooling and exhumation by *c.* 195 Ma (Hansen *et al.*, 1991). White mica compositions of DC-109 and DC-111 are consistent with igneous crystallization, as supported by field, petrographic and geochemical data. These rocks, as well as a mica quartzite (DC-112), then experienced high-P/T ductile shear. Ductile shear accompanying high-P/T metamorphism is suggested by the preservation of a population of igneous white mica. This requires deformation and metamorphism in an environment which would allow some of the white mica grains to recrystallize with a composition reflecting equilibrium with new P–T conditions, yet preserve other white mica grains of igneous composition. White mica in DC-112 also records a ductile deformation at low-P not evident in the structurally continuous orthogneisses DC-109 and DC-111. DC-112 has a relatively uniform, fine grain size, and it lacks mechanically robust minerals, such as plagioclase or K-feldspar, which might 'protect' mica from strain, and hence chemical recrystallization. In contrast, orthogneisses DC-109 and DC-111 are coarse grained, with a range of mineral sizes, and contain plagioclase and K-feldspar. More data are needed to resolve these questions; however, it appears that white mica preserves a record of three distinct P–T environments.

This has important implications for the effect of shear strain on mineral composition. White mica composition in paragneiss and orthogneiss L-S tectonites may be useful in constraining the P–T conditions of ductile deformation, as well as the P–T path. These data also indicate that care should be taken in applying thermobarometric study to dynamically recrystallized rocks.

In summary, TSZ tectonites record high-P/T prograde metamorphism, and retrogression which accompanied the change from D_{Nds} to D_{Dss} deformation. Cassiar tectonites also record high P–T conditions, although an overall lower pressure is indicated.

P–T–TIME–DISPLACEMENT PATHS

Combining the above P–T constraints with previously documented structural and kinematic (Hansen, 1989b) and thermochronometric histories (Hansen *et al.*, 1989, 1991) results in P–T–time–displacement paths for tectonites within the study area. The rocks are treated here as two different packages: (1) TSZ tectonites, between the d'Abbadie and Big Salmon faults and in klippen east of the d'Abbadie fault; and (2) Cassiar tectonites east of, and including, the d'Abbadie fault zone. P–T, time–T, and P–time diagrams annotated with displacement data are illustrated for each package (Fig. 11). I can determine only a few points along a particular P–T–time path and the sequence of these points. The path between any two points is constrained by both geological and geochronological considerations. The tectonic histories of TSZ and Cassiar tectonites are discussed separately below, followed by a discussion of their common evolution.

TSZ tectonites

Ductilely deformed and variably metamorphosed rocks of the TSZ are comprised of three lithotectonic assemblages (Tempelman-Kluit, 1979): (1) an assemblage with affinity to oceanic sedimentary strata, which includes metamorphosed chert, argillite, carbonate and graphitic siltstone; (2) an assemblage characteristic of oceanic crust, including massive to pillowed basalt, gabbro and ultramafic rock; and (3) an assemblage which may represent a volcano-plutonic arc, including felsic gneiss and continentally derived(?) sedimentary strata. The TSZ evolved as a zone of high strain, and is divisible into three domains on the basis of kinematic history, D_{Nds}, D_{Dss} and D_{Rds} from west to east (Hansen, 1989b).

P–T–time–displacement paths constructed for the TSZ (Fig. 11a–c) include *P–T*–time data from eclogite and blueschist enclosed in Teslin-Taylor Mountain and Nisutlin tectonites. TSZ tectonites follow a clockwise *P–T* path that mimics a trench geotherm, similar to prograde paths of circum-Pacific and Alpine–Himalayan high-*P* belts which record subduction zone metamorphism. Tectonites show a progressive increase in temperature at *c.* 245 Ma to a maximum of 750° C, coincident with pressure increase to form blueschist, eclogite and high-*P* amphibolite (Fig. 11b, c). Not every TSZ tectonite reached the peak *P–T* conditions recorded by the TSZ as a whole, nor did all tectonites reach their thermal or baric peak at the same time. For example, blueschist which records Permian cooling (Ermder & Armstrong, 1988) reached a peak temperature of 400° C and cooled through this temperature by 250 Ma (Fig. 11b), whereas D_{Nds} tectonite LV-197AB reaches higher peak metamorphic conditions (*c.* 575° C, >9 kbar) yet did not cool through 350° C until 195 Ma (Hansen *et al.*, 1991). The highest *P–T* conditions are recorded in D_{Nds} tectonites (575–750° C and 9–14 kbar), similar to conditions derived from enclosed eclogite which record hysteretic *P–T* paths (Erdmer & Helmstaedt, 1983). D_{Dss} deformation occurred under lower *P–T* conditions (400–550° C and 5–8 kbar). D_{Rds} tectonites record a peak temperature of *c.* 420° C and minimum peak pressure of 3 kbar. Normal, or west-side down displacement accompanied the highest pressure conditions, and was followed by strike-slip displacement at lower *P–T* conditions. As evidenced by concordant $^{40}Ar/^{39}Ar$ plateau cooling dates, the TSZ was exhumed quickly as a coherent structural block in early Jurassic time. TSZ tectonite quartz grains typically show flat-field extinction and straight boundaries indicative of latent heating and annealing following deformation; hence deformation probably did *not* accompany rapid cooling, but rather, pre-dated rapid cooling. If deformation had accompanied rapid cooling one would expect to observe highly strained quartz (ribbons, undulatory extinction, ragged boundaries) rather than the observed annealed quartz. D_{Rds} tectonites were also most likely metamorphosed and deformed *prior* to fast exhumation of D_{Nds} and D_{Dss} tectonites in the early Jurassic because quartz grains in these rocks also show typical flat-field extinction and straight boundaries indicative of annealing following the end of deformation. If D_{Rds} tectonism accompanied, rather than pre-dated, early Jurassic cooling one would have to explain how these rocks were annealed following deformation.

TSZ tectonites record evidence of widespread high-*P*/*T* metamorphism accompanied by penetrative ductile deformation within a coherent metamorphic belt *c.* 15–20 km wide and greater than 60 km long. Evidence of high-*P*/*T* metamorphism is not limited to locally preserved lensoids of eclogite. D_{Nds} tectonites which enclose eclogite themselves record high *P–T* conditions. The general lack of retrogression of D_{Nds} tectonites may reflect metamorphism in a non-collisional subduction zone (cf. Ernst, 1988). D_{Nds} conditions are similar to those recorded by high-*P* amphibolite of the Catalina Schist, California (Platt, 1975; Sorensen, 1986; Bebout & Barton, 1989). D_{Dss} tectonites record a retrograde path from higher-*P*/*T* D_{Nds} deformation which accompanied local dextral strike-slip displacement. The inverted metamorphic gradient of D_{Nds}, D_{Dss} and D_{Rds} is consistent with metamorphism within a west-dipping subduction zone in which material was progressively underplating to the upper plate during subduction (cf. Peacock, 1987). The tectonite fabric of each of these three domains may result from progressive underplating of material from the subduction channel (Cloos & Shreve, 1988) to the base of the upper plate during subduction (Hansen, 1991). With continued subduction and underplating the upper plate–subduction channel boundary may have migrated trenchward resulting in 'growth' of the upper plate at depth. TSZ tectonites preserved a record of progressive backflow, dextral margin-parallel shear, and downflow within the subduction channel as recorded by D_{Nds}, D_{Dss} and D_{Rds} tectonites, respectively (Hansen, 1992). The lower *P–T* conditions may reflect a change in position within the subduction zone as a result of subduction zone-parallel translation, or collision with continental crust. The former explanation explains better the mineral fabrics and is favoured.

Cassiar tectonites

Cassiar tectonites record a quite different tectonic history (Fig. 11d–f). Peraluminous orthogneiss intruded in Devonian–Early Carboniferous time. Emplacement *P–T* conditions, derived from white mica, are consistent with plutonism within either a volcanic arc or a rift environment. Following igneous crystallization, Cassiar rocks experienced static cooling (Fig. 11e). Cassiar orthogneiss and paragneiss later experienced penetrative top-to-the-east ductile shear deformation under increasingly higher pressure, as recorded by the range in orthogneiss white mica compositions (Fig. 11f). A prograde high-*P–T* path is consistent with white mica compositions, and with garnet core–rim compositions. Following prograde dynamothermal metamorphism these tectonites cooled slowly under static conditions (Fig. 11e, f). Locally, along the trace of the d'Abbadie fault, these tectonites were sheared and ductilely deformed at depth in middle Cretaceous time.

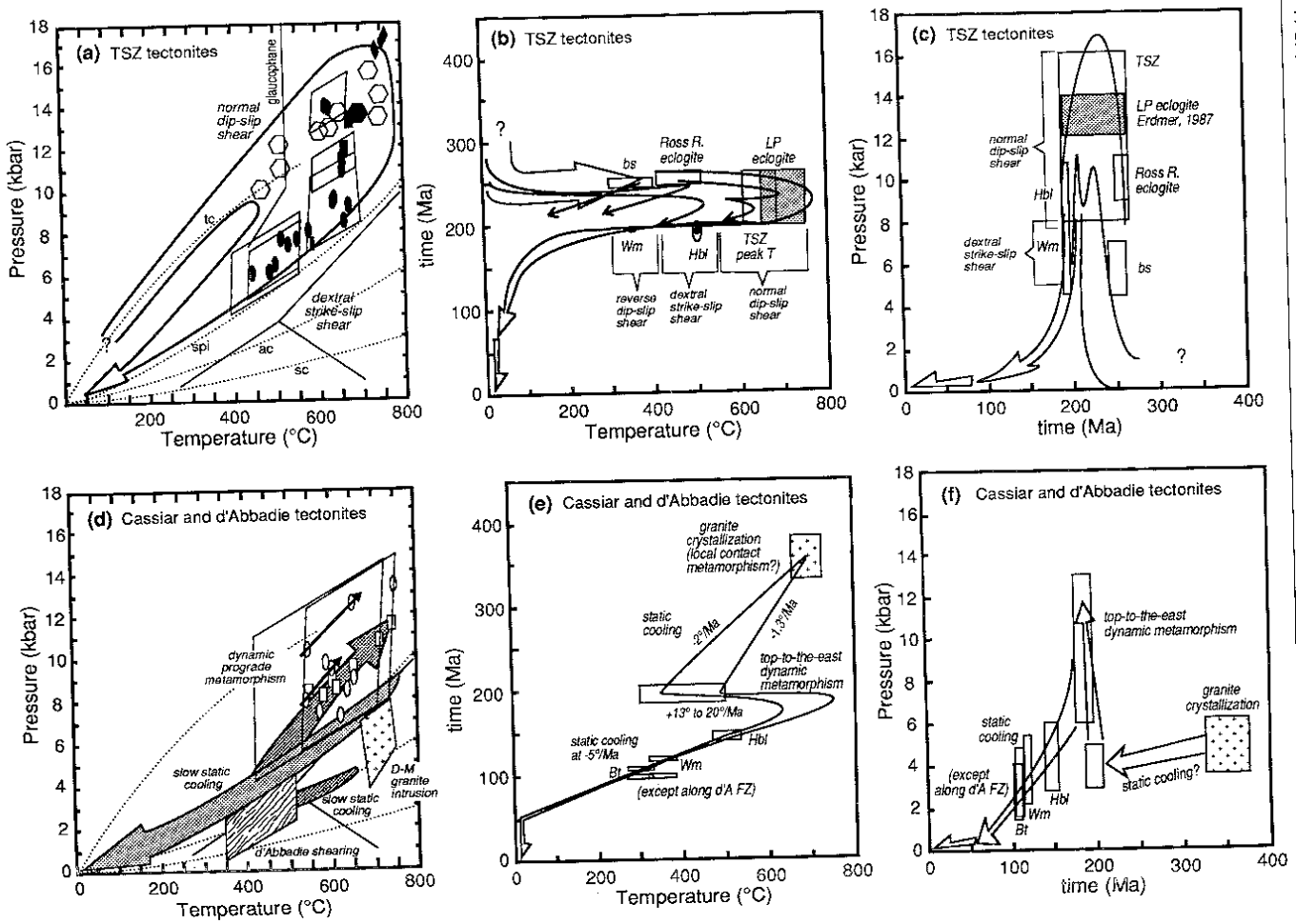
(a) TSZ tectonites
normal dip-slip shear
dextral strike-slip shear
spl
ac
sc
tc
Pressure (kbar)
Temperature (°C)
(b) TSZ tectonites
Ross R. eclogite
LP eclogite
bs
Wm
Hbl
TSZ peak T
reverse dip-slip shear
dextral strike-slip shear
normal dip-slip shear
time (Ma)
Temperature (°C)
(c) TSZ tectonites
TSZ
LP eclogite Erdmer, 1987
Ross R. eclogite
normal dip-slip shear
dextral strike-slip shear
Hbl
Wm
bs
Pressure (kar)
time (Ma)
(d) Cassiar and d'Abbadie tectonites
dynamic prograde metamorphism
slow static cooling
D-M granite intrusion
slow static cooling
d'Abbadie shearing
Pressure (kbar)
Temperature (°C)
(e) Cassiar and d'Abbadie tectonites
granite crystallization (local contact metamorphism?)
static cooling
2°/Ma
1.3°/Ma
top-to-the-east dynamic metamorphism
+13° to 20°/Ma
static cooling at ~5°/Ma
Hbl
Wm
Bt
(except along d'A FZ)
time (Ma)
Temperature (°C)
(f) Cassiar and d'Abbadie tectonites
top-to-the-east dynamic metamorphism
granite crystallization
static cooling
(except along d'A FZ)
Hbl
Wm
Bt
static cooling?
Pressure (kbar)
time (Ma)

Cassiar tectonites were also locally heated and statically metamorphosed along the borders of middle Cretaceous plutons (Spicuzza & Hansen, 1989; Smith & Erdmer, 1990).

Cassiar tectonites record slow static cooling through 500–300° C from *c.* 145 to 110 Ma. Projecting this cooling rate (*c.* 6° C Ma^{-1}) back from 500° C at 145 Ma (Hbl, $^{40}Ar/^{39}Ar$) on the *T*–time diagram to *c.* 700° C (*c.* peak metamorphic temperature of Cassiar tectonites) implies heating of Cassiar rocks from *c.* 400° C at 195 Ma to 700° C at 185 Ma (Fig. 11e), consistent with ductile deformation accompanying prograde metamorphism as described above. An increase in pressure is required (Fig. 11e), consistent with overthrusting of TSZ tectonites, and resultant top-to-the-east imbrication of Cassiar tectonites. The Cassiar tectonite package cooled slowly through 300° C by 109 Ma, consistent with a lack of ductile deformation accompanying retrograde metamorphism or cooling. The depth of emplacement for the Late Cretaceous Nisutlin batholith (Spicuzza & Hansen, 1989) falls along the *P–T* curve projected in Fig. 11(f). Cassiar and TSZ tectonites both deformed in a ductile fashion at depth during dextral movement along the d'Abbadie fault. Ductile deformation probably lasted through 97 Ma at the level of d'Abbadie L-S tectonites currently exposed. Muscovite and biotite from dextral S-C orthogneiss adjacent to the fault yielded a $^{40}Ar/^{39}Ar$ plateau cooling date of 97 Ma. These data further support slow cooling of Cassiar tectonites in middle to Late Cretaceous time (Fig. 11e). Granitic plutons intruded Cassiar tectonites and the d'Abbadie fault zone in middle to Late Cretaceous time (Tempelman-Kluit, 1979; Gabrielse, 1985; Armstrong, 1988). Cassiar tectonites east of the d'Abbadie fault are interpreted to have continued to cool and to be exhumed at a relatively continuous rate, reaching the surface at approximately 60 Ma.

The following relations indicate that the major deformation and metamorphism of Cassiar L-S tectonites is not related to middle Cretaceous plutonism: (1) *P–T* conditions of Cassiar tectonism show a higher *P/T* gradient than modern volcano-plutonic arcs, and they lie along or above a stable plate interior gradient; (2) top-to-the-east L-S tectonite fabrics preserved in Cassiar tectonites are cut by the Dycer stock, a middle Cretaceous pluton; (3) Cassiar tectonites show no increase in metamorphic grade adjacent to the Dycer stock; (4) Cassiar tectonites that record top-to-the-east shear fabrics are thermally overprinted within 1 km of the middle Cretaceous Nisutlin batholith (Fig. 1; Spicuzza & Hansen, 1989); (5) Cassiar metamorphism pre-dates middle Cretaceous plutonism—although Cassiar tectonites record peak metamorphic temperatures up to 750° C, $^{40}Ar/^{39}Ar$ data indicate that these tectonites cooled through 500° C by 145 Ma, and through 300° C by 109 Ma, whereas K–Ar mica cooling dates for the plutons generally range from 100 to 75 Ma (Tempelman-Kluit 1979; Gabrielse, 1985; Armstrong, 1988).

I interpret that ductile shear recorded in Cassiar tectonites resulted from top-to-the-east overthrusting of TSZ tectonites. Chattermarks preserved locally at the base of TSZ klippen record top-to-the-east displacement (Erdmer, 1985) and Cassiar tectonites record top-to-the-east ductile shear (Hansen, 1989a; Spicuzza & Hansen, 1989). TSZ tectonics record rapid cooling through 300–500° C at *c.* 195 Ma, interpreted as the time of exhumation resulting from collision, and interpreted as the initiation of Cassiar ductile deformation as a result of underthrusting. As TSZ tectonites were exhumed and cooled through 300° C in early Jurassic time, lower-plate Cassiar tectonites could be expected to have undergone amphibolite facies deformation. TSZ deformation is interpreted as B-type subduction, whereas Cassiar tectonism is interpreted as A-type subduction.

Tectonic implications

TSZ and Cassiar tectonites record different high *P–T* metamorphism. TSZ tectonites record a complex dip-slip and strike-slip displacement history which accompanied clockwise high-*P/T* metamorphism along a trench geotherm, and cooled quickly as a coherent block in early Jurassic time. In contrast, Cassiar tectonites record prograde dynamothermal metamorphism along a shallower *P/T* gradient accompanied by east-vergent shearing, followed by static cooling in middle Jurassic through Cretaceous time. In addition, the protoliths of the two assemblages are different; the overthrust assemblage is oceanic and ocean margin material, whereas the underthrust assemblage is continental material.

TSZ ductile deformation is compatible with the calculated thermobarometry. Temperatures are higher than those typically inferred for blueschist terranes.

Fig. 11. *P–T, P–t, T–t* plots for tectonite packages (a–c) TSZ and (d–f) Cassiar. (a) *P–T* plot. Dotted lines mark average geothermal gradients for trench (tc), stable plate interior (spi), arc complex (ac), and spreading centre (sc) (after Ernst, 1976). *P–T* constraints from this study are shown in addition to constraints from eclogite (hexagons) from Teslin-Taylor Mountain and Nisutlin tectonites in Yukon (Erdmer, 1987). The filled hexagon represents the eclogite from the northern TSZ transect (Fig. 2). Other eclogite localities are shown in Fig. 1. (b) *t–T* plot. Blueschist (bs) and eclogite dates from Ross River area (Erdmer & Armstrong, 1988) record cooling of individual tectonites; hornblende and white mica $^{40}Ar/^{39}Ar$ dates (Hansen *et al.*, 1991) record final cooling of the TSZ through 500 and 350° C, respectively. Thin arrows represent possible, but not unique, paths; eclogites record helical paths (Erdmer & Helmstaedt, 1983). Final exhumation is constrained by volcanic rocks which locally overlie TSZ-correlative tectonites (Armstrong, 1988). (c) *P–t* plot. Constraints are as discussed for (a) and (b). (d) *P–T* plot. Dotted lines as in (a). *P–T* constraints from this study are shown. Thin arrows represent core–rim trends. (e) *t–T* plot. Granite crystallization from U–Pb (zircon; Hansen *et al.*, 1989). Static cooling to *c.* 200 Ma is assumed (see text). Hornblende, white mica and biotite $^{40}Ar/^{39}Ar$ dates (Hansen *et al.*, 1991) indicate slow cooling. Final exhumation is constrained by the projection of the cooling curve determined by hornblende, white mica and biotite dates, and is consistent with volcanic rocks which overlie Cassiar tectonites (Armstrong, 1988). (f) *P–t* plot. Constraints as stated for (d) and (e). See text for discussion.

Therefore, TSZ rocks must have been deformed in a hot portion of a subduction complex. Although several factors govern temperature profiles in subduction systems, two of these provide a means by which metamorphism can take place at relatively high temperature. The highest temperature within a subduction complex is along the hangingwall of the overriding plate. Slow subduction rates allow relaxation of depressed geotherms, and could allow for somewhat elevated temperatures in the subduction complex. Metamorphic P–T data reported here, however, indicate a low gradient (*c.* 19° C km^{-1}) which is compatible with a subduction environment. Unusual gradients produced by slow convergence rates are thus unlikely. TSZ tectonites probably formed close to the hangingwall plate, and were progressively underplated to it.

If TSZ tectonites were underplated to the hangingwall plate, the distribution of metamorphic facies may provide a key to the polarity of the subduction zone. Lower-grade tectonites in the east and higher-grade tectonites in the west suggest an inverted metamorphic gradient and west-dipping subduction. The interpretation is supported by numerous regional relations (Tempelman-Kluit, 1979; Erdmer, 1985; Hansen, 1988; Mortensen, 1991).

The subduction zone is interpreted to have formed by at least pre-middle to Late Permian time based on K–Ar muscovite and Rb–Sr dates of 259–249 Ma from blueschist and eclogite (Erdmer & Armstrong, 1988) (Fig. 12). Hence, TSZ tectonites represent a subduction zone active as early as 250 Ma with subduction continuing for ≥50 Ma from middle Permian to Early Jurassic time (195 Ma). Assuming a moderate orthogonal convergence rate of 50 km Ma^{-1}, approximately 2500 km of oceanic crust could reasonably be consumed along this boundary (Tempelman-Kluit, 1979) (this estimate would be reduced to *c.* 1800 km for a similar rate along a boundary with 45° of obliquity).

B-type subduction apparently ceased in early Jurassic time as the leading edge of western North American continental crust was subducted (Fig. 12). TSZ tectonites were uplifted as a coherent block as a result of the collision. North American (and Cassiar) strata were imbricated along east-vergent thrust faults, and underwent high-P/T metamorphism as a result.

Evidence presented here corroborates the suggestion that Devonian–Early Carboniferous orthogneisses and their host metasedimentary rocks (Fig. 1) are tectonically equivalent to the underthrust Cassiar terrane (Hansen, 1990; Dusel-Bacon & Hansen, 1991; Hansen *et al.*, 1991). That is, both packages represent the leading edge of subducted Permo-Triassic North American continental crust, and are exposed as structural windows.

CONCLUSIONS

Mineral compositions and thermobarometry indicate that the TSZ represents a coherent belt of high-P/T tectonites metamorphosed along a trench geotherm. The highest

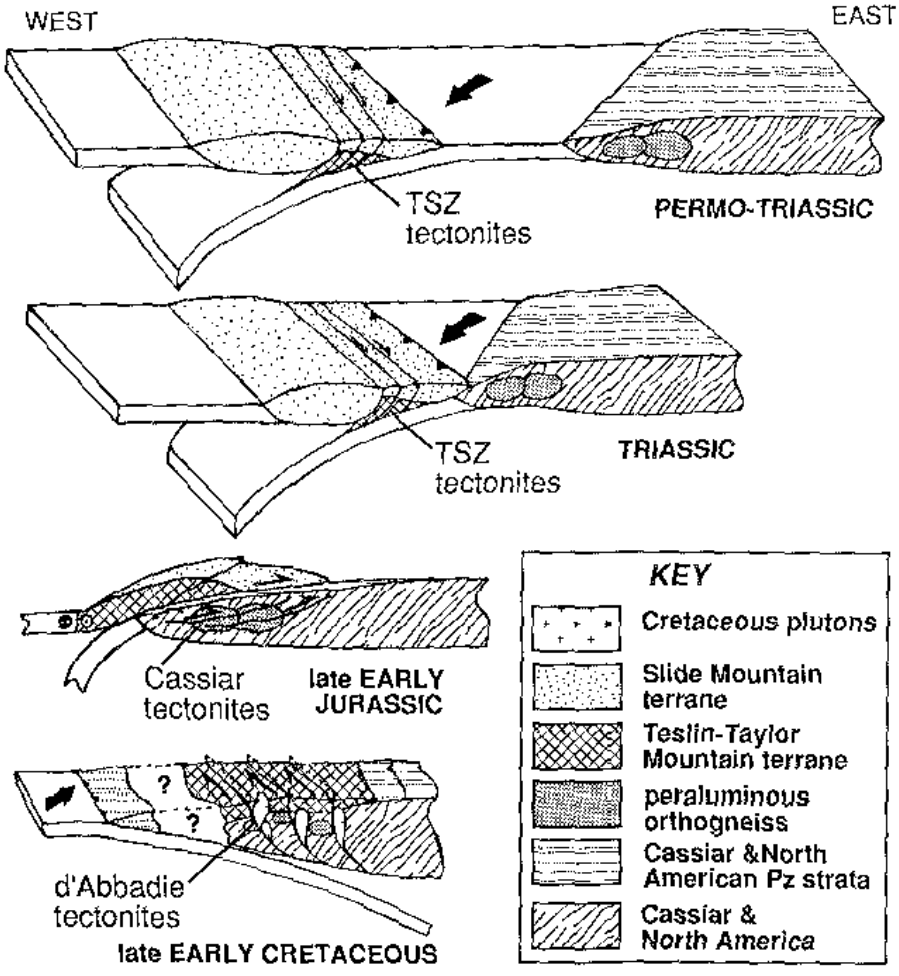

Fig. 12. Schematic diagrams of the tectonic setting of TSZ, Cassiar and d'Abbadie tectonites (modified from Hansen, 1990; Hansen *et al.*, 1991).

P–T conditions are recorded in D_{Nds} tectonites (575–750° C and 9–17 kbar), similar to conditions recorded by enclosed eclogite blocks. D_{Dss} deformation occurred under lower P–T conditions (400–550° C and 5–8 kbar). D_{Rds} tectonites record a temperature of *c.* 420° C and minimum pressure of 3 kbar. Dynamothermal metamorphism ended prior to cooling in early Jurassic time. Cassiar tectonites record top-to-the-east prograde metamorphism at moderate-P, high-T conditions (550–750° C and 7–13 kbar) along or above a stable plate interior geotherm. Following metamorphism Cassiar tectonites cooled slowly through 500–300° C in middle Jurassic and middle Cretaceous time.

Tectonically, the TSZ represents the deep-seated portion of a west-dipping Permo-Triassic subduction complex. TSZ tectonites were underplated to the upper plate during B-type subduction. Subducted material was, in part, underplated to the upper plate during downflow and backflow. With continued subduction and underplating the hangingwall–subduction channel boundary migrated basinward resulting in 'growth' of the upper plate at depth. Following basin collapse, TSZ tectonites were uplifted as a coherent structural package in early Jurassic time during, and as a result of, A-type subduction of North American and Cassiar strata. Cassiar strata were dynamothermally metamorphosed as a result of underthrusting; this metamorphism of these rocks pre-dates, and is not directly related to, later widespread middle Cretaceous plutonism. Underthrust North American continental crust in southern Yukon cooled slowly as a result of exhumation due to erosion. Both underthrust and overthrust assemblages were dissected by middle Cretaceous dextral strike-slip faults and plutons.

TSZ, Cassiar, and d'Abbadie tectonites were deformed during changing P–T conditions, Data from each of these tectonite packages indicates that grain-scale strain partitioning may have allowed local recrystallization of individual minerals, white mica in particular, by the addition of mechanical energy. The composition of each new grain may reflect the P–T conditions under which that particular grain was deformed.

ACKNOWLEDGEMENTS

This work was supported by the Exploration and Geological Services Division of DIANA, Whitehorse, Yukon, by National Science Foundation Grants (EAR85-07953 and EAR-8715911), and by the Department of Earth and Space Sciences, University of California, Los Angeles, in the form of a graduate research fellowship. Acknowledgement is also made to the donors of The Petroleum Research Fund, administered by the American Chemical Society, for partial support of this research. Many people have contributed to my understanding during numerous discussions; in particular I thank P. Choukroune, W. G. Ernst and J. W. Goodge. I am grateful to P. Erdmer, J. W. Goodge, M. J. Holdaway and L. S. Hollister for reviews of the manuscript. All errors or misinterpretations remain my responsibility.

REFERENCES

Albee, A. L. & Ray, L., 1970. Correction factors for electron probe microanalysis of silicates, oxides, carbonates, phosphates, and sulfates. *Analytical Chemistry*, **42,** 1408–1414.

Anovitz, L. M. & Essene, E. J., 1982. Phase relations in the system $CaCO_3$–$MgCO_3$–$FeCO_3$. *Eos, Transactions of the American Geophysical Union*, **63,** 464.

Apted, M. J. & Liou, J. G., 1983. Phase relations among greenschist, epidote-amphibolite, and amphibolite in a basaltic system. *American Journal of Science*, **283-A,** 328–354.

Armstrong, R. A., 1988. Mesozoic and early Cenozoic magmatic evolution of the Canadian Cordillera. *Geological Society of America Special Paper*, **218,** 55–91.

Ashworth, J. R. & Evirgen, M. M., 1985. Plagioclase relations in pelites, central Menderes Massif, Turkey. II. Perturbation of garnet-plagioclase geobarometers. *Journal of Metamorphic Geology*, **3,** 219–229.

Bally, A. W., 1981. Thoughts on the tectonics of folded belts. In: *Thrust & Nappe Tectonics* (eds McClay, K. & Price, N. J.), pp. 13–32. Blackwell Scientific Publications, London.

Bebout, G. E. & Barton, M. D., 1989. Fluid flow and metasomatism in a subduction zone hydrothermal system: Catalina Schist terrane, California. *Geology*, **17,** 976–980.

Bell, T. H., 1985. Deformation partitioning and porphyroblast rotation in metamorphic rocks: a radical reinterpretation. *Journal of Structural Geology*, **3,** 109–118.

Bell, T. H. & Hammond, R. L., 1984. On the internal geometry of mylonite zones. *Journal of Geology*, **92,** 667–686.

Bennett, V. C. & Hansen, V. L., 1988. Neodymium isotopic similarities between the Yukon-Tanana terrane, Yukon Territory and continental North America. *Geological Society of America Abstracts with Programs*, **20,** A111.

Boulter, C. A. & Råheim, A., 1974. Variations in Si^{4+} content of phengites through a three stage deformation sequence. *Contributions to Mineralogy and Petrology*, **48,** 57–71.

Brown, E. H., 1977. The crossite content of Ca-amphibole as a guide to pressure of metamorphism. *Journal of Petrology*, **18,** 53–72.

Chopin, C. & Maluski, H., 1980. $^{40}Ar/^{39}Ar$ dating of high pressure metamorphic micas from the Gran Paradiso Area (western Alps): evidence against the blocking temperature concept. *Contributions to Mineralogy and Petrology*, **74,** 109–122.

Cloos, M. & Shreve, R. L., 1988. Subduction-channel model of prism accretion, melange formation, sediment subduction, and subduction erosion at convergent plate margins: 1. Background and description. *Pure and Applied Geophysics*, **128,** 454–489.

Dusel-Bacon, C. & Hansen, V. L., 1991. High-P, medium-T metamorphism and ductile deformation during Early Mesozoic convergence of two subterranes of the Yukon-Tanana composite terrane (YTT), eastern Alaska. *Geological Society of America Abstracts with Programs*, **22,** 20.

Erdmer, P., 1985. An examination of the cataclastic fabrics and structures of parts of Nisutlin, Anvil and Simpson allochthons, central Yukon: test of the arc–continent collision model. *Journal of Structural Geology*, **7,** 57–72.

Erdmer, P., 1987. Blueschist and eclogite in mylonitic allochthons, Ross River and Watson Lake areas, southeastern Yukon. *Canadian Journal of Earth Sciences*, **24,** 1439–1449.

Erdmer, P. & Armstrong, R. L., 1988. Permo-Triassic isotopic dates for blueschist, Ross River area, Yukon. In: *Yukon Geology*, Vol. **2,** pp. 33–36. Indian and Northern Affairs, Whitehorse.

Erdmer, P. & Helmstaedt, H., 1983. Eclogite from central Yukon: a record of subduction at the western margin of ancient North America. *Canadian Journal of Earth Sciences*, **20,** 1389–1408.

Ernst, W. G., 1963. Petrogenesis of glaucophane schists. *Journal of Petrology*, **4,** 1–30.

Ernst, W. G., 1975. Systematics of large-scale tectonics and age progressions in Alpine and circum-pacific blueschist belts.

Tectonophysics, **26**, 229–246.
Ernst, W. G., 1976. *Petrologic Phase Equilibria*. Freeman and Co., San Francisco, 333 pp.
Ernst, W. G., 1988. Tectonic history of subduction zones inferred from retrograde blueschist P-T paths. *Geology*, **16**, 1081–1084.
Essene, E. J., 1982. Geologic thermometry and barometry. In: *Characterization of Metamorphism Through Mineral Equilibria* (ed. J. M. Ferry), pp. 153–207. Mineralogical Society of America.
Ferry, J. M. & Spear, F. S., 1978. Experimental calibration of the partitioning of Fe and Mg between biotite and garnet. *Contributions to Mineralogy and Petrology*, **66**, 113–117.
Frey, M., Hunziker, J. C., Jager, E. & Stern, W. B., 1983. Regional distribution of white K-mica polymorphs and their phengite content in the Central Alps. *Contributions to Mineralogy and Petrology*, **83**, 185–197.
Gabrielse, H., 1985. Major dextral transcurrent displacements along the Northern Rocky Mountain Trench and related lineaments in north-central British Columbia. *Geological Society of America Bulletin*, **96**, 1–14.
Ganguly, J., 1979. Garnet and clinopyroxene solid solutions and geothermometry based on Fe–Mg distribution coefficient. *Geochimica et Cosmochimica Acta*, **43**, 1021–1029.
Ghent, E. D. & Stout, M. Z., 1981. Geobarometry and geothermometry of plagioclase–biotite–garnet–muscovite assemblages. *Contributions to Mineralogy and Petrology*, **76**, 92–97.
Goldman, D. S. & Albee, A. L., 1977. Correlation of Mg/Fe partitioning between garnet and biotite with O^{18}/O^{16} partitioning between quartz and magnetite. *American Journal of Science*, **277**, 750–767.
Goldsmith, J. R. & Heard, H. C., 1961. Sub-solidus phase relations in the system $CaCO_3$–$MgCO_3$. *Journal of Geology*, **69**, 45–74.
Goldsmith, J. R. & Newton, R. C., 1969. P-T-X relations in the system $CaCO_3$–$MgCO_3$ at high temperatures and pressures. *American Journal of Science*, **267A**, 160–190.
Gordey, S. P., 1981. Stratigraphy, structure and tectonic evolution of southern Pelly Mountains in the Indigo Lake area, Yukon Territory. *Geological Survey of Canada Bulletin*, **318**, 44.
Gordey, S. P., Gabrielse, H. & Orchard, M. J., 1982. Stratigraphy and structure of Sylvester Allochthon, southwest McDame map area, northern British Columbia. *Current Research, Part B, Geological Survey of Canada Paper*, **82-1B**, 101–106.
Graf, D. F. & Goldsmith, J. R., 1955. Dolomite–magnesian calcite relations at elevated temperatures and CO_2 pressures. *Geochimica et Cosmochimica Acta*, **7**, 109–128.
Graham, C. M. & Powell, R., 1984. A garnet–hornblende geothermometer: calibration, testing, and application to the Pelona Schist, southern California. *Journal of Metamorphic Geology*, **2**, 13–31.
Guidotti, C. V. & Sassi, F. P., 1976. Muscovite as a petrogenetic indicator mineral in pelitic schists. *Neues Jahrbuch für Mineralogie Abhandlungen*, **127**, 97–142.
Hansen, V. L., 1987. Structural, metamorphic, and geochronologic evolution of the Teslin suture zone, Yukon: evidence for Mesozoic oblique convergence outboard of the northern Canadian Cordillera. *Unpubl. PhD Thesis, University of California, Los Angeles*.
Hansen, V. L., 1988. A model for terrane accretion: Yukon-Tanana and Slide Mountain terranes, northwest North America. *Tectonics*, **7**, 1167–1177.
Hansen, V. L., 1989a. Mesozoic evolution of the Yukon-Tanana terrane. *Geological Society of America Abstracts with Programs*, **21**, 90.
Hansen, V. L., 1989b. Structural and kinematic evolution of the Teslin suture zone, Yukon: record of an ancient transpressional margin. *Journal of Structural Geology*, **11**, 717–733.
Hansen, V. L., 1990. Yukon-Tanana terrane: a partial acquittal. *Geology*, **18**, 365–369.
Hansen, V. L., 1992. Deep-seated backflow, margin-parallel shear, and downflow within an ancient subduction complex. *Geology*, in press.
Hansen, V. L., Armstrong, R. L. & Mortensen, J. K., 1989. Pre-Jurassic ductile deformation and synchronous metamorphism of the Yukon-Tanana terrane: geochronologic constraints from the Teslin suture zone, Yukon. *Canadian Journal of Earth Sciences*, **26**, 2224–2235.
Hansen, V. L., Heizler, M. T. & Harrison, T. M., 1991. Mesozoic thermal evolution of the Yukon-Tanana terrane, Yukon and Alaska: new evidence from $^{40}Ar/^{39}Ar$ data. *Tectonics*, **10**, 51–76.
Harms, T. A., 1985. Pre-emplacement thrust faulting in the Sylvester allochthon, northeast Cry Lake map area, British Columbia. *Geological Survey of Canada Paper*, **85-1A**, 301–304.
Hodges, K. V. & Crowley, P. D., 1985. Error estimation and empirical geothermobarometry for pelitic systems. *American Mineralogist*, **70**, 702–709.
Hodges, K. V. & Spear, F. S., 1982. Geothermometry, geobarometry and the Al_2SiO_5 triple point at Mt. Moosilauke, New Hampshire. *American Mineralogist*, **67**, 1118–1134.
Hoisch, T. D., 1990. Empirical calibration of six geobarometers for the mineral assemblage quartz + muscovite + biotite + plagioclase + garnet. *Contributions to Mineralogy and Petrology*, **104**, 225–234.
Holdaway, M. J., 1971. Stability of andalusite and the aluminum silicate phase diagram. *American Journal of Science*, **271**, 97–131.
Jacobson, C. E., 1984. Petrological evidence for the development of refolded folds during a single deformation event. *Journal of Structural Geology*, **6**, 563–570.
Kohn, M. J. & Spear, F. S., 1990. Empirical calibration of geobarometers for the assemblage garnet–hornblende–plagioclase–quartz. *American Mineralogist*, **75**, 89–96.
Laird, J. & Albee, A. L., 1981a. High-pressure metamorphism in mafic schist from northern Vermont. *American Journal of Science*, **281**, 97–126.
Laird, J. & Albee, A. L., 1981b. Pressure, temperature, and time indicators in mafic schist: their application to reconstructing the polymetamorphic history of Vermont. *American Journal of Science*, **281**, 127–175.
Liewing, N., Caron, J.-M. & Clauer, N., 1981. Geochemical and K–Ar isotopic behavior of Alpine sheet silicates during polyphase deformation. In: *The Effect of Deformation on Rocks* (eds Lister, G. S., Behr, H.-J., Weber, K. & Zwart, H. J.), *Tectonophysics*, **78**, 273–290.
Maruyama, S., Suzuki, K. & Liou, J. G., 1983. Greenschist–amphibolite transition equilibria at low pressures. *Journal of Petrology*, **24**, 583–604.
Massone, H.-J. & Schreyer, W., 1987. Phengite geobarometry based on the limiting assemblage with K-feldspar, phlogopite, and quartz. *Contributions to Mineralogy and Petrology*, **96**, 212–224.
Miyashiro, A., 1961. Evolution of metamorphic belts. *Journal of Petrology*, **2**, 277–311.
Mortensen, J. K., 1983. Age and evolution of the Yukon-Tanana terrane, southeastern Yukon Territory. *Unpubl. PhD Thesis, University of California, Santa Barbara*.
Mortensen, J. K., 1991. Pre-mid-Mesozoic tectonic evolution of the Yukon-Tanana terrane, Yukon and Alaska. *Tectonics*, in press.
Nelson, J. L., 1990. The Blue Dome fault: a fossil transform fault in the Sylvester allochthon. *Geological Association of Canada Program with Abstracts*, **15**, A95.
Nelson, J. & Bradford, J., 1987. Geology of the area around the Midway deposit, northern British Columbia (104O/16). *British Columbia Ministry of Energy, Mines and Petroleum Resources, Geological Fieldwork, 1986*, **1987-1**, 181–192.
Nelson, J., Bradford, J. A., Green, K. C. & Marsden, H., 1988. Geology and patterns of mineralization, Blue Dome map area, Cassiar district (104P/12). *British Columbia Ministry of Energy,*

Mines and Petroleum Resources, Geological Fieldwork, 1987, **1988-1**, 233–243.

Orville, P. M., 1972. Plagioclase cation exchange equilibria with aqueous chloride solution: results at 700° C and 2000 bars in the presence of quartz. *American Journal of Science*, **272**, 947–955.

Peacock, S. M., 1987. Creation and preservation of subduction-related inverted metamorphic gradients. *Journal of Geophysical Research*, **92**, 12763–12781.

Perkins, D., III, Essene, E. J. & Marcotty, L. A., 1982. Thermometry and barometry of some amphibole-granulite facies rocks from the Otter Lake area, southern Quebec. *Canadian Journal of Earth Sciences*, **19**, 1759–1774.

Platt, J. P., 1975. Metamorphic and deformational processes in the Franciscan Complex, California: some insights from the Catalina Schist terrane. *Geological Society of America Bulletin*, **86**, 1337–1347.

Powell, R., Condliffe, D. M. & Condliffe, E., 1984. Calcite–dolomite geothermometry in the system $CaCO_3$–$MgCO_3$–$FeCO_3$: an experimental calibration. *Journal of Metamorphic Geology*, **2**, 33–41.

Rasse, P., 1974. Al and Ti contents of hornblende, indicators of pressure and temperature of regional metamorphism. *Contributions to Mineralogy and Petrology*, **45**, 231–236.

Roddick, J. A., 1967. Tintina trench. *Journal of Geology*, **75**, 23–33.

Saliot, P. & Velde, B., 1982. Phengite compositions and post-nappe high-pressure metamorphism in the Pennine zone of the French Alps. *Earth and Planetary Science Letters*, **57**, 133–138.

Smith, J. M. & Erdmer, P., 1990. The Anvil aureole, an atypical mid-Cretaceous culmination in the northern Canadian Cordillera. *Canadian Journal of Earth Sciences*, **27**, 344–356.

Sorensen, S. S., 1986. Petrologic and geochemical comparison of the blueschist and greenschist units of the Catalina Schist terrain, southern California. In: *Blueschists and Eclogites* (eds Evans, B. W. & Brown, E. H.), *Geological Society of America Memoir*, **164**, 59–75.

Spear, F. S., 1981. An experimental study of hornblende stability and compositional variability in amphibole. *American Journal of Science*, **281**, 697–734.

Spear, F. S., 1990. *Program manual and computer exercises for the calculation of metamorphic phase equilibria, pressure–temperature–time paths and thermal evolution of orogenic belts.* Geological Society of America Short Course Notes.

Spicuzza, M. J. & Hansen, V. L., 1989. Constraints on Mesozoic evolution of south-central Yukon: structural and metamorphic data from the Late Cretaceous Nisutlin batholith and host rocks. *Geological Society of America Abstracts with Programs*, **21**, 147.

Tempelman-Kluit, D. J., 1970. An occurrence of eclogite near Tintina trench, Yukon. *Geological Survey of Canada Paper*, **70-1B**, 19–22.

Tempelman-Kluit, D. J., 1979. Transported cataclasite, ophiolite and granodiorite in Yukon: evidence of arc–continent collision. *Geological Survey of Canada Paper*, **79-14**, 27 pp.

Thompson, A. B., 1976. Mineral reactions in pelitic rocks. II. Calculations of some P–T–X (Fe–Mg) phase relations. *American Journal of Science*, **276**, 425–454.

Velde, B., 1967. Si content of natural phengites. *Contributions to Mineralogy and Petrology*, **14**, 250–258.

Wheller, J. O., Brookfield, A. J., Gabrielse, H., Monger, J. W. H., Tipper, H. W. & Woodsworth, G. J., 1988. Terrane map of the Canadian Cordillera. *Geological Survey of Canada Open File*, **1894**, scale, 1:2,000,000.

Received 16 April 1991; revision accepted 23 August 1991.